2017

Ellipsometric Measurements of Alternative Fuels

Leigh Nash
University of Central Florida

ELLIPSOMETRIC MEASUREMENTS OF ALTERNATIVE FUELS

by

LEIGH NASH
B.S. University of Central Florida, 2014

A thesis submitted in partial fulfillment of the requirements
for the degree of Master of Science
in the Department of Mechanical and Aerospace Engineering
in the College of Engineering and Computer Science
at the University of Central Florida
Orlando, Florida

Summer Term
2017

Major Professor: Subith Vasu

ABSTRACT

Alternative jet fuels will be important in the future to ensure cleaner burning, reliable, and reasonably priced air transportation. One important property that must meet certification standards is the fuel's thermal stability, or its ability to withstand heating before breaking down. Jet fuels are used as engine coolants, and thermally unstable fuels can form deposits in the fuel delivery systems, leading to a loss of fuel flow.

In the past, the thermal stability of a fuel was rated using a color standard method. The color of the deposit left on a metal tube that had been heated and exposed to a test fuel were matched with a color standard to rate the level of deposition, and thus the fuel's thermal stability. Ellipsometry, which is an optical technique that uses changes in a beam of light's polarization after it reflects off a sample to determine the thickness of any film on that sample, has recently been implemented to improve the thermal stability characterization standard.

Various aspects of the ellipsometric method have been investigated in this work. In addition, several thermal stability studies were carried out. The effect of increasing temperature on the thermal stability of Sasol Iso-Paraffinic Kerosene, Jet A, JP-8, and Gevo jet fuel have been analyzed, and the effect of varying levels of the additive naphthalene in Sasol IPK has also been investigated. Various theoretical optical models have been evaluated for their ability to predict deposit thickness. Finally, attempts to validate these measurements were made using scanning electron microscopy, ellipsometric tube rating, interferometric tube rating, and reference tubes. The analysis carried out in this work was used to make recommendations for improving the thermal stability test standard.

Dedicated to everyone who helped me on this journey.

ACKNOWLEDGMENTS

This work is supported by the National Aeronautics and Space Administration under Grant Number NNX15AU28H issued through the NASA Education Minority University Research Education Project (MUREP) through the NASA Harriett G. Jenkins Graduate Fellowship activity.

I would like to thank Henry Homann, Michelle Sestak, and Celine Eypert from Horiba Scientific for their assistance in setting up the ellipsometer and their advice on the optical models. I would additionally like to thank Tim Ubienski, Joy Buehler, and Terry McCue from the NASA Glenn Research Center Analytics group for their assistance in performing the SEM data collection and analysis. I would like to thank Zachary West and Tim Edwards from Wright Patterson Air Force Base in Dayton Ohio for their collaboration on parts of this work, including the ETR and ITR sections.

I would also like to acknowledge the various members of my lab group for their help, support, and friendship throughout this experience. I would like to thank Joseph Lopez, Zach Loparo, Erik Ninnemann, Sam Barak, Owen Pryor, Batikan Koroglu, Akshita Parupalli, Sneha Neupane, Mike Villar, and Kyle Thurmond.

Finally, I would like to thank my mentor from NASA Glenn Research Center, Jennifer Klettlinger, and my advisor Dr. Vasu. Their support, advice, and guidance will always be appreciated.

TABLE OF CONTENTS

LIST OF FIGURES

LIST OF TABLES

LIST OF ACRONYMS

A = Height of the peak of the ε_i curve in the Tauc-Lorentz dispersion

ASTM = American Society for Testing and Materials

ATJ = Alcohol to Jet

c = Speed of light in a vacuum

C = Full width at half maximum of the peak of the ε_i curve in the Tauc-Lorentz dispersion

E = Photon energy in the Tauc-Lorentz dispersion

E_0 = Photon energy of the peak of the ε_i curve in the Tauc-Lorentz dispersion

E_g = Photon energy at which the ε_i curve is first nonzero in the Tauc-Lorentz dispersion

EDS = Energy Dispersive x-ray Spectroscopy

ETR = Ellipsometric Tube Rater

eV = Electron volts

f_j = Height of j^{th} peak of the coefficient of extinction curve in the New Amorphous dispersion

f = Frequency of light

GC = Gas Chromatography

h = Planck's constant

HLPS = Hot Liquid Process Simulator

IPK = Iso Paraffinic Kerosene

ITR = Interferometric Tube Rater

JFTOT = Jet Fuel Thermal Oxidation Test

k = Coefficient of extinction

N = Complex index of refraction

n = Index of refraction

NJFCP = National Jet Fuel Combustion Program

n_∞ = Value of the index of refraction as photon energy of the incoming light approaches infinity in the New Amorphous dispersion

R^p = Total reflectance coefficient in the direction parallel to the light propagation direction

R^s = Total reflectance coefficient in the direction perpendicular to the light propagation direction

$r_{ij}^{p,s}$ = Reflectance coefficient between the i^{th} and j^{th} surface in the parallel or perpendicular direction respectively

SEM = Scanning Electron Microscopy

t = Thickness

v = Speed of light in a particular material

WPAFB = Wright Patterson Air Force Base

β = Phase change through one layer of film

Δ = Phase change across the sample

ε = Dielectric function

ε_i = Imaginary part of the dielectric function

ε_r = Real part of the dielectric function

ε_∞ = Value of the ε_r curve as the photon energy of the incident light approaches infinity in the Tauc-Lorentz dispersion

Γ_j = The full width at half maximum of the j^{th} peak of the coefficient of extinction curve in the New Amorphous dispersion

λ = Wavelength

ϕ = Angle between the light beam and the sample normal

Ψ = Ratio of the total reflectance coefficients

χ^2 = Goodness of fit parameter

ω = Photon energy in the New Amorphous dispersion

ω_g = Photon energy at which the coefficient of extinction is first nonzero in the New Amorphous dispersion

ω_j = Photon energy of peak of the coefficient of extinction curve in the New Amorphous dispersion

CHAPTER ONE: INTRODUCTION

The world's energy demands are only increasing with time. In the aviation sector, much of the energy comes from petroleum oil sources, however alternative fuels are becoming increasingly important because they are cleaner burning than traditional fuels in many cases, and can be produced in a variety of ways. 11 percent of greenhouse gas emissions produced by the transportation sector in the United States come from aviation [1]. In addition, these emissions are produced mostly at higher altitudes, where they have more of a greenhouse effect than they would at ground level. Many of the issues currently facing the aviation community can be remedied using alternative fuels. In addition to being cleaner burning than their traditional counterparts, many come from renewable sources such as plant stock. Alternative fuels can also be made from gasified coal, which is an abundant natural resource in the United States [2]. Many agencies, including NASA, are interested in alternative fuels for these reasons.

Before an alternative fuel can be certified for use in flight, it must be rigorously and thoroughly tested. It is often desirable for these fuels to be used as direct, or drop in, replacements for traditional fuels, meaning that they are used in engines that were designed to run on traditional fuels without modification to the engine hardware [1]. This can only be accomplished with extensive testing to determine how the fuel and engine will interact in every conceivable aspect. Such testing is done according to the American Society for Testing and Manufacturing (ASTM) standards. The overall standards that define the procedures for alternative jet fuel certification are ASTM D4054-14 "Standard Practice for Qualification and Approval of New Aviation Turbine Fuels and Fuel Additives" [3], and ASTM D7566 "Standard Specification for Aviation Turbine Fuel Containing Synthesized Hydrocarbons [4]." Thermal stability is characterized according to

ASTM D3241 “Standard Test Method for Thermal Oxidation Stability of Aviation Turbine Fuels” [5] which is referenced in the previously mentioned standards.

Development and certification of alternative jet fuels according to these standards is very expensive and time consuming. This means that it can take several years for new fuels to be accepted and used in actual engines. The National Jet Fuel Combustion Program (NJFCP) was formed with the goals of streamlining the certification of alternative fuels and standardizing their testing. The NJFCP is a partnership between research universities, industry, and the federal government. This program aims to develop better chemical models for alternative fuels, validate those models with various experimental tests, and develop a standard test rig for fuel certification. The partners want to reduce the enormous time and monetary investments that must be made to develop and certify alternative fuels. Primary characteristics of interest to the NJFCP are a fuel’s lean blow out limit, altitude relight, and cold start properties [1].

The NJFCP defines the combustor fuel coking properties of a fuel as a “secondary feature of merit,” which includes the fuel’s thermal stability. Thermal stability refers to a fuel’s ability to withstand thermal stressing, or the degree to which it breaks down as it is heated. In addition to being used as the propellant, the fuel is also often used as engine coolant to save weight and space inside the aircraft, particularly in military applications. As it flows through the cooling channels absorbing heat from the engine, the fuel heats up and may begin to break down if thermally unstable. This can lead to clogging of fuel lines, nozzles, and injectors, and a loss of fuel flow. This behavior is called coking or fouling. The fouling process is roughly analogous to the way a person’s arteries can become blocked with plaque over their lifetime leading to a loss of blood flow. It is also important to know the fuel’s thermal stability properties in order to anticipate

maintenance schedules, to know when components might need to be cleaned or replaced, and to avoid unnecessary down time.

Thermal stability is inherently difficult to define directly, and thus even more difficult to measure. Stability is generally defined indirectly by measuring a change in a related property, such as deposition. Originally, it was defined using a color standard according to ASTM D3241 [5]. The fuel of interest was flowed at a defined rate over an aluminum tube that had been heated to a particular test temperature (see Chapter 3 for details). Then, any deposit left on the tube was compared to the color standard, which defines ten color levels (0, <1, 1, <2, 2, <3, 3, <4, 4, and >4) as shown below in Figure 1. A color rating of 0 corresponds to a clean tube, and the colors get progressively darker as the rating number increases. The logic behind this is that darker colors indicate thicker deposits, and less thermally stable fuels. A rating of 3 or below is considered passable thermal stability, and <4 or above are considered failing ratings.

Figure 1: ASTM color standard used in thermal stability testing

There are however, numerous issues with this method. It has been demonstrated that the color standard rating is quite non-repeatable and subjective to the operator of the test [6]. Because a person must visually inspect the tube and compare it to the standard, the accuracy of the test is limited by the accuracy of the person's eyes and their perception of color. In addition, this color standard is only applicable to aluminum tubes and traditional fuels, which limits the tests that can be performed. Many other metals are used in aircraft engines, including stainless steel, so it is advantageous to have a test method that is not sensitive to the substrate type. Also, alternative fuels can leave different color deposits than traditional fuels, and the rating given by the color standard may not be reflective of the fuel's actual thermal stability in these cases. The color standard test yields only qualitative data about the thermal stability of the fuel. The color levels are quite broad, and very different fuels can receive the same stability rating. These facts make it difficult to draw detailed conclusions about a fuel, or about any of its components. Finally, the physical comparison standard can fade over time if not stored properly, leading to increased uncertainty in the results of the test.

This has led to the implementation of ellipsometry as a method for measuring the thermal stability of jet fuels. At the time of this writing, ellipsometry is included in the appendix to the test method as a valid alternative to the color standard. Ellipsometry is an optical technique that uses changes in the intensity and phase of light reflected from a sample to determine the thickness of a film on the sample surface (see Chapter 3 for details). The tubes are prepared according to the same procedure that is required for the color standard test. Point measurements can be taken along the length of the tube and around its circumference to generate a thickness profile from the individual measurements.

Ellipsometry improves over all of the inadequacies of the color standard method. It yields objective numerical data that is repeatable. This method can be applied to any tube material and fuel combination. In addition, it is very detailed and precise. Small changes in the deposit thickness are detectable using ellipsometry, allowing for detailed fuel investigations to be performed. These same types of analyses are not possible using the color standard method as a large amount of detail is lost when only the color rating is considered.

Tested Fuels

Various fuels were tested in this work, including Sasol IPK, Gevo, Jet-A, and JP-8. Varying levels of naphthalene in the Sasol IPK were also considered. Sasol IPK is an isoparaffinic kerosene fuel produced by Sasol. This fuel is greater than 90 percent C_{10} and C_{12} isoparaffins, which is much more pure than traditional fuels, which typically have hundreds or even thousands of components. A typical Sasol IPK fuel is made up of 2.6 percent cycloparaffins and 97.4 percent normal and isoparaffins [7] [8]. This fuel is produced using the Fischer-Tropsch process from gasified coal [9]. The first step in the Fischer-Tropsch process is to gasify the coal to produce syn-gas. The syn-gas is then converted to crude oil and then separated into usable fuels. Paraffin wax, an olefin light oil, and water are produced through the following reaction steps [10].

$$2H_2 + CO \rightarrow CH_2 + H_2O \tag{1}$$

$$(2n+1)H_2 + nCO \rightarrow C_nH_{2n+2} + nH_2O \tag{2}$$

$$2nH_2 + nCO \rightarrow C_nH_{2n} + nH_2O \quad (3)$$

$$CO + H_2O \leftrightarrow CO_2 + H_2 \quad (4)$$

Equation 1 is the global Fischer-Tropsch reaction, Equation 2 is the paraffin producing reaction, Equation 3 produces the olefins, and Equation 4 is the water gas shift reaction. A comparison of Sasol IPK with Jet A is shown in Table 1. The Sasol IPK is mostly iso-paraffins by percentage mass, while the Jet A has a more even distribution among the iso, normal, and cyclo paraffins and aromatics.

Table 1: Compositional comparison of Sasol IPK and Jet A

Fuel	Iso-paraffins (mass%)	Normal paraffins (mass%)	Cyclo-paraffins (mass%)	Aromatics (mass%)
Sasol IPK	89	2	8	<1
Jet A	29	20	32	17

A gas chromatography analysis of Sasol IPK is shown in Figure 2. The gas chromatography and fuel compositional analysis for all the fuels studied here was performed by Tim Edwards and Linda Shafer at Wright Patterson Air Force Base. There are not many peaks in this chart, indicating that this fuel has few components. This is advantageous because it makes the effects of the components on the thermal stability easier to discern. This also makes this fuel easier to model, and it is less likely to vary from batch to batch.

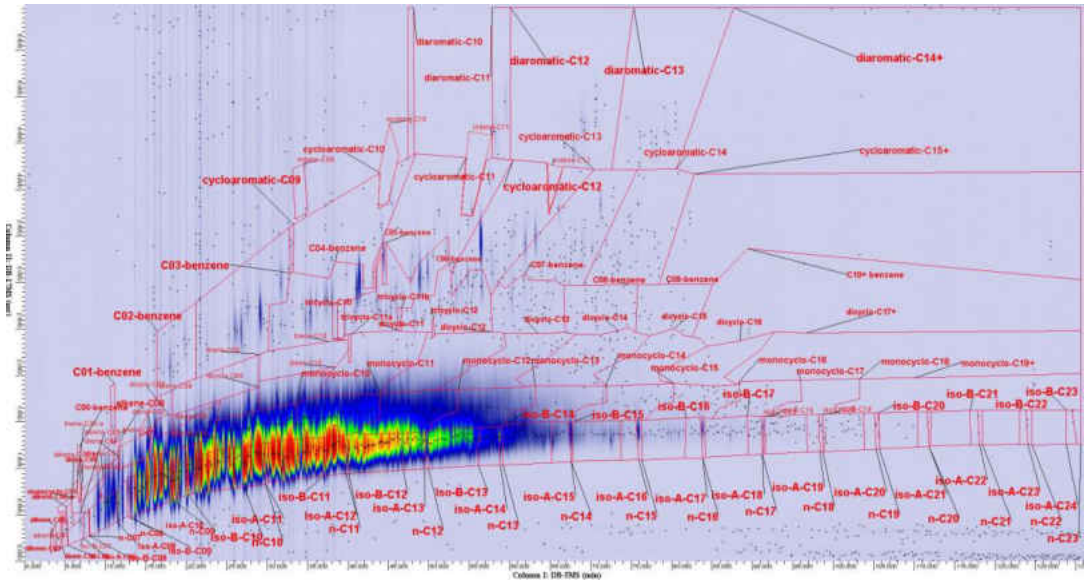

Figure 2: GC analysis of Sasol IPK [Tim Edwards and Linda Shafer]

Naphthalene is two-ringed aromatic additive (see Figure 3) used to improve the fuel's autoignition performance for safety purposes. Aromatics generally increase a fuel's ignition delay time because energy input is required to break the bonds in the aromatic's rings. Naphthalene has the chemical formula $C_{10}H_8$ and it used to be the primary component in mothballs before it was found to be too harmful for household use. There is anecdotal evidence suggesting that adding naphthalene mothballs to a car's gas tank will improve fuel performance, but will also gum up the engine components, suggesting a negative impact on thermal stability.

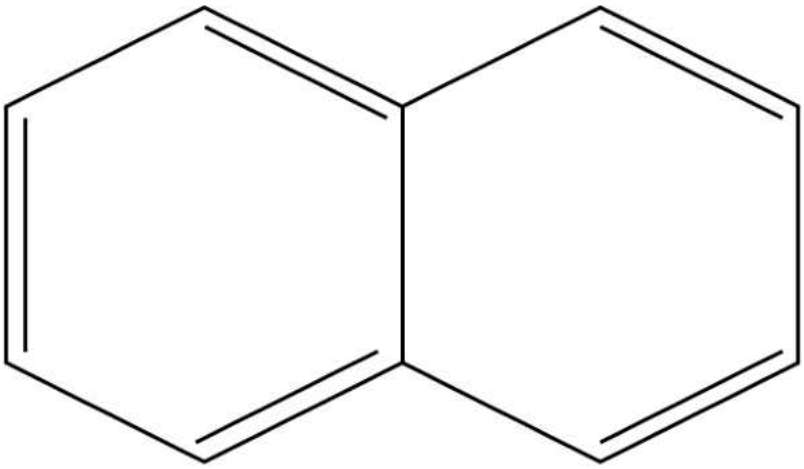

Figure 3: Naphthalene structure

Gevo, an alcohol-to-jet (ATJ) fuel was also investigated in this work. A GC analysis of this fuel is shown in Figure 4. This fuel has the fewest components of all the fuels tested here, as evidenced by this figure. Gevo is isobutanol ($C_4H_{10}O$) made from plant derived feedstock, and it is 99.43 percent isoparaffins by weight, 0.02 percent normal paraffins, 0.54 percent normal paraffins, and 0.01 percent aromatics. Again, credit and thanks are given to Tim Edwards and Linda Shafer at WPAFB for the compositional analysis of the fuels. This fuel is even more heavily weighted towards the isoparaffins than the Sasol IPK.

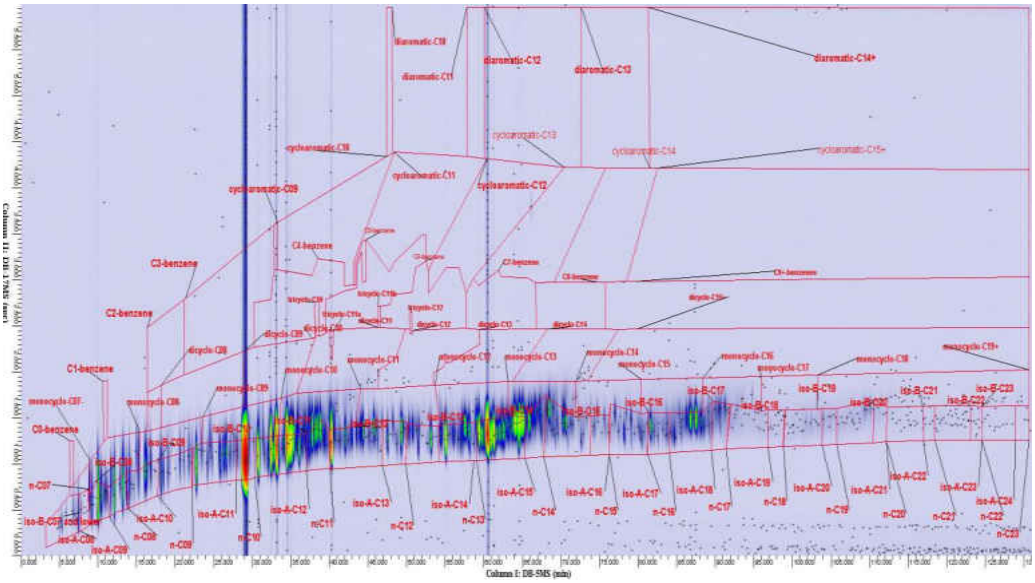

Figure 4: GC analysis of Gevo fuel [Tim Edwards and Linda Shafer]

Jet A and JP-8 are traditional kerosene based fuels. Alternative fuels are often used in mixtures with traditional fuels to make the alternatives easier to use as drop in replacements. A GC analysis of a kerosene based fuel similar to a traditional jet fuel is shown in Figure 5 that can be compared with the ones shown in Figure 2 and Figure 4. The greater number of peaks here indicates that the traditional fuels have many more components than the alternative fuels. Jet A is the most commonly used commercial jet fuel in the United States, and JP-8 is the most commonly used fuel by the US military.

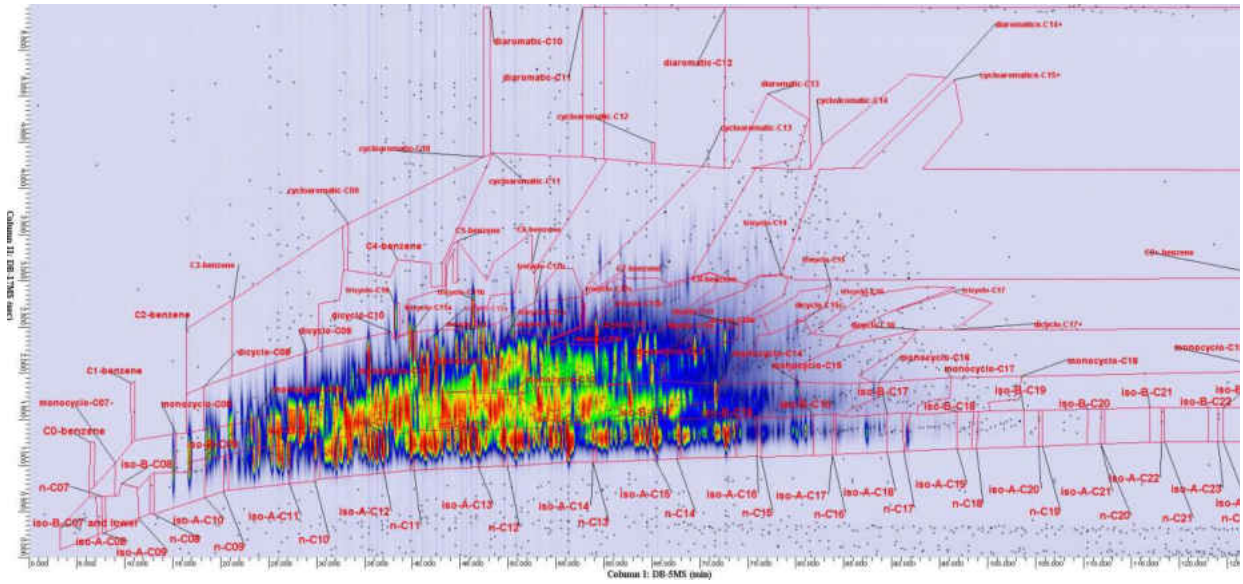

Figure 5: GC analysis of a typical kerosene fuel [Tim Edwards and Linda Shafer]

Table 2 shows a comparison of the Sasol IPK fuel to Jet A and JP-8. All three have approximately equal hydrogen content by mass, but the Sasol IPK has a much lower percentage by volume of aromatics and percentage by mass of sulfur. These two points are important because aromatics and sulfur are both known to drastically reduce a fuel's thermal stability, even in small amounts. Because of this, it is expected that the two traditional fuels will be less thermally stable than the Sasol IPK.

Table 2: Alternative and traditional fuel composition comparison

Fuel	Aromatics (volume%)	Total Sulfur (mass%)	Hydrogen Content (mass%)
Sasol IPK	0.5	<0.001	15.1
Jet A	18.7	0.21	14.09
JP-8	16.5	0.06	13.8

The goal of this work is to first test the thermal stability of alternative fuels and the effect of additives and substrate types using ellipsometry. Other goals include providing a commentary

on the effectiveness of this method because it is still not widely used. There is a very high barrier to the adoption of ellipsometry because of the expensive equipment required to perform the analysis and the initial learning curve that must be overcome, so the adoption process has been slow so far. The hope is that successful uses will encourage others to implement this method. Finally, the thermal stability testing standards are currently under review, so suggestions are made to improve the method.

CHAPTER TWO: LITERATURE REVIEW

Many different techniques have been tried to quantify a fuel's thermal stability and deposition behavior. These include quartz crystal microbalances, carbon burn off analysis, oxygen sensors, and various devices made specifically to be used in the JFTOT.

A quartz crystal microbalance and single tube flow reactor system were used by Corporan et al [11] to evaluate the thermal stability of various alternative fuels. This technique involves directly weighing deposits, and would be difficult to implement for thinner deposits, such as the ones investigated in this work. A quartz crystal microbalance was also used by Zabarnick [12] to assess the thermal stability of jet fuel at 140 °C at atmospheric pressure and low oxygen availability, simulating the actual operating conditions of an engine. One batch of Jet A-1 was tested in addition to two batches of Jet A. One was hydrotreated and the other was not.

Carbon burn off can also be used to analyze thermal oxidation deposits. In their 2004 work, JP-8 was heated to 500 °C and flowed over metal surfaces in an isothermal flow reactor by Altin et al [13] at 34 atm for 5 hours. Nickle, 304 and 316 stainless steel, Silcosteel, and glass lined stainless steel tubes were tested, and it was found that the nickel surfaces had the most deposition, followed by the 316-stainless steel, 304 stainless steel, Silcosteel, and finally the glass-lined stainless steel. Deposition was quantified using a carbon analyzer, which oxidized the deposit and measured the amount of CO_2 produced. The deposits were also examined using a scanning electron microscope. This type of analysis has the benefit of being able to directly measure the mass of the deposit, but it destroys the sample, which prevents further testing from being done.

Jet fuel deposits were created on flat metal surfaces using a modified JFTOT Flat Sample Rig by Lauer et al [14] at temperatures around 250 °C. Strips of aluminum, stainless steel, and

silver foil were used. Jet A, dodecane, and an experimental reference fuel with broadened properties were investigated. Varying levels of several additives including thiophene, furan, pyrrole, copper, and iron naphthenates were tested. Spectroscopic FTIR emission data was taken. It was found that fuel composition, temperature, boundary conditions, and concentration of nonhydrocarbon species had an effect on the oxidation rate of the fuel, which was described as the primary deposition mechanism.

Turbulent flow devices called the Navy Aviation Fuel Thermal Stability Simulator, and the High Reynolds Number Thermal Stability bench rig were compared by Pande et al [15] to two laminar flow devices called the Tubular Reactor and a bench device designed by the Naval Air Systems Command were compared in terms of their ability to predict a fuel's thermal stability. The thermal stability was assessed based on carbon burn off of the deposits, and good correlation was found between the two, suggesting that laminar tests such as the JFTOT adequately predict a fuel's thermal stability. Nine fuels were tested including one batch of JP-8, five batches of JP-5, one Jet A, and a diesel fuel.

An isothermal oxidation apparatus with an oxygen sensor was used by Grinstead et al [16] to measure the oxidation and deposition rates of jet fuel. Three batches of JP-5 and four of Jet A were analyzed with varying levels of sulfur, copper, and iron and from various suppliers.

The effect of various components on thermal stability have been studied. Usually these studies focus on classes of species, such as antioxidants, or peroxides. Hydroperoxide decomposing species alone in a jet fuel were found by Zabarnick [17] to have no effect on oxidation at 140 °C. The addition of a phenolic species in addition to the hydroperoxide decomposing species was found to slow oxidation. A quartz crystal microbalance was used to quantify the level of oxidation. Exxsol D110 solvent, Jet A-1, and Jet A were tested.

Thermally stressed jet fuels and surrogates were analyzed theoretically by Heneghan et al [18] and it was found that decreasing oxygen concentration lead to less deposition, and easily oxidized fuels were found to be more stable.

Jet A and JP-8 samples were examined with and without anti-oxidant after storage by Bessee et al [19]. The Jet A with antioxidant added was found to have very high storage stability. The findings of this study show that antioxidant should be added to fuels for storage stability purposes either at the refinery or after they have been transported. Total acid number, peroxide number, and the JFTOT breakpoint according to the color standard were tested and reported.

Attempts have been made to create chemical kinetic models to describe deposit formation. Mechanisms for the breakdown of jet fuels are discussed by Altin et al [20]. One possibility is that an oxidation reaction occurs uniformly throughout the free-flowing fuel, creating particles that become the deposits seen on engine surfaces. Another is a reaction that occurs only at the sections of the flow that interact with the metal surfaces, with the metals catalyzing the reaction. Sulfur may also act as a catalyst.

A chemical kinetic model to simulate the autoxidation of jet fuels was created and tested at temperatures around 200 °C by Zabarnick [21]. This model shows that antioxidants are important in slowing oxidation and that alkyl hydroperoxide breakdown is important in fuel oxidation.

Several studies have looked at the effect of thermal stability on alternative fuels, including synthetic paraffinic kerosenes like the Sasol IPK tested in this work. No studies on Gevo were found. The properties of three alternative fuels were assessed by Wilson [19] after storage at conditions that mimic long term storage for use by the military. The fuels were a FT SPK, HEFA SPK, and B20. Various additives were included in the fuel and their effects were noted. An

ellipsometer was used to assess the fuels' thermal stability, and in several cases, it was noted where thick invisible deposits were formed at unexpected temperature locations on the heated tubes. Deposits were formed at lower temperature spots on the tubes rather than the traditional downstream point of the maximum temperature.

The JFTOT color standard was used to measure the thermal break temperature of a Fischer-Tropsch fuel with varying levels of aromatics by Klettlinger [22]. Color test results indicated that the aromatics had a negative impact on the thermal stability of the fuel, but it was unclear if there was actually more deposit present in these cases, and ellipsometry was mentioned as a possible continuation of this work.

Jet A-1 and a Fischer-Tropsch fuel were investigated by Edwards et al [23] at supercritical pyrolytic conditions in a flow reactor, and it was found that the Fischer-Tropsch fuel was more reactive and formed more deposits. Various methods were employed to determine the composition of the fuels and deposits including high pressure liquid chromatography, gas chromatography, mass spectrometry, and flame ionization detection.

In the early 1990s Ellipsometry was used by Baker et al [6] to measure the deposition of several Merox fuels and to determine the effect of increasing temperature and test time on the thermal break point of the fuel. Ellipsometry was compared to the visual rating procedure and x-ray diffraction. Similar deposit increase trends with temperature were observed to those presented in this work, where the deposit increases slowly up to a specific temperature and then at a much quicker rate.

The thermal stability of JP-8 was assessed using a spectroscopic ellipsometer over the temperature range from 255 to 275 C by Browne et al [24], and the results were compared to the

color standard test. A modified JFTOT procedure was used, and the tubes were exposed to the fuel using a hot liquid process simulator. The work presented here is a follow on to these results.

CHAPTER THREE: METHODOLOGY

This chapter details the optical properties that make the method of ellipsometry possible, the equipment used in this study, and the optical models investigated for determining deposit thicknesses.

Polarization

Ellipsometry uses the changes in the polarization of a beam of light after it reflects off of a sample to determine characteristics of that sample. A beam of light can be broken into two components: one oscillating perpendicularly to the beam's direction of travel, and one oscillating parallel to the direction of travel. Polarization is defined by the relative amplitudes and phases of these components. All units of polarized light have the same polarization, while non-polarized light contains units with differing polarizations. The logic behind the naming convention for polarization types can be understood by imagining the wave of light as a series of rays with the originating point of each ray located on the midpoint of the wave, and the end point of the ray changing amplitude and direction to follow the height of the wave [25]. The components of linearly polarized light are in phase with each other. If the imaginary rays are viewed normal to the direction in which the light is propagating, they will fall on a line, hence the term linear polarization. This is shown visually in Figure 6.

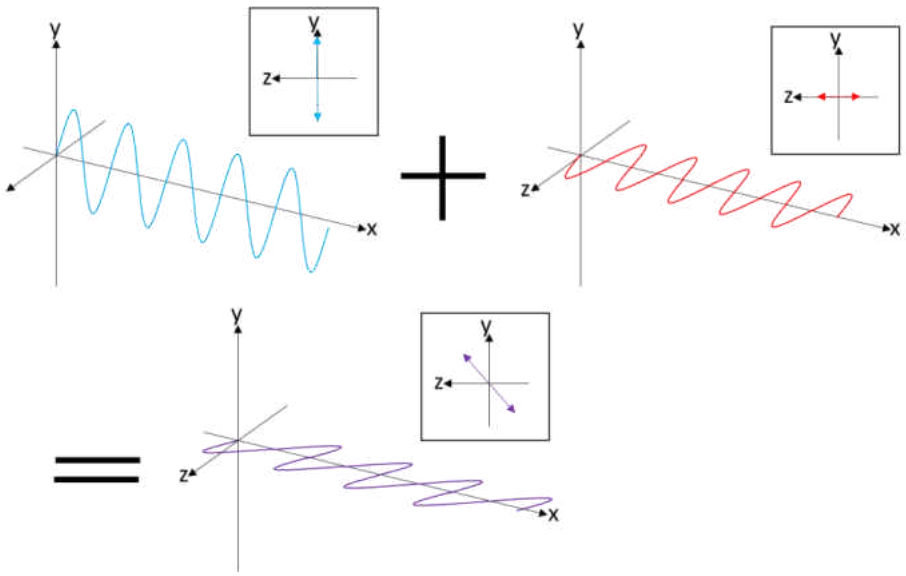

Figure 6: Polarization visualization

The components of circularly polarized light are exactly 90 degrees out of phase with each other and have equal amplitudes. The rays in this case trace out a circle. Elliptically polarized light has components that are out of phase by an arbitrary amount and have arbitrary amplitudes. These rays trace out an ellipse, and ellipsometry is named for its use of elliptically polarized light. Reflection from a surface can change the polarization of a beam of light [25].

Ellipsometric Principles

When light encounters the boundary between two different materials, a portion of the light reflects and a portion refracts as shown in Figure 7. This is governed by Snell's law [25], given by Equation 5.

$$n_0 \sin \varphi_i = n_1 \sin \varphi_t \tag{5}$$

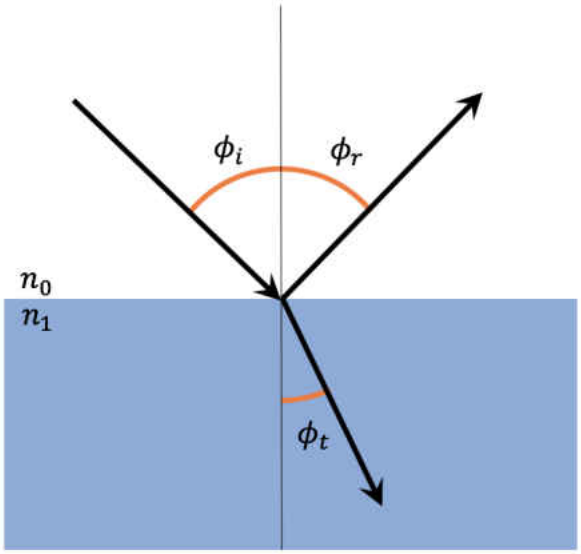

Figure 7: Behavior of light at an interface

Snell's law is dependent on the materials' index of refraction (n), which is a ratio of the speed of light in a vacuum to the speed of light in that material (see Equation 6 where c is the speed of light in a vacuum and v is the speed of light in the material), and the angle of the incident light with respect to the sample normal, ϕ_i. ϕ_i is also equal to the angle of the reflected light to the sample normal, ϕ_r. These two angles are equal because the reflected light does not change mediums, meaning that the index of refraction does not change, so Snell's law dictates that the angles must be the same.

$$n = \frac{c}{v} \tag{6}$$

ϕ_t is the angle of the transmitted, or refracted light to the sample normal. The angle of the refracted light can be determined when the angle of incidence and the indices of refraction of the two materials are known. Another important material parameter to the interaction between the light and the sample is the coefficient of extinction (k), which determines how quickly the light entering the material is absorbed [25].

If a sample has multiple layers (see Figure 8), the reflection and refraction behavior described above occur at each interface [25]. The naming convention shown in Figure 8 will be followed throughout this section to explain the interaction between the light and the layered sample.

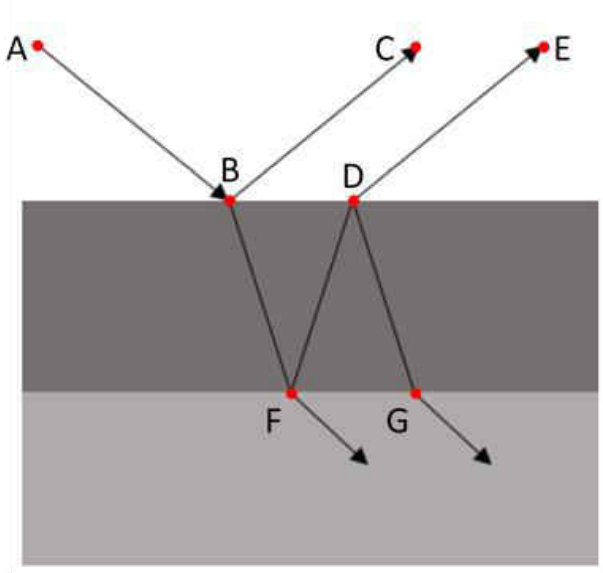

Figure 8: Multi-layer sample

The layers in Figure 8 are representative of the layers investigated on the physical tube samples. It is helpful to imagine the sample in this way to aid in the modeling process, which will be described in detail in the following sections. The white layer represents the ambient above the deposit and tube, the dark gray layer is the deposit left by the heated jet fuel, and the light gray layer is the substrate, which is the tube itself. The substrate is modeled as an infinitely thick layer because all of the light entering it is absorbed. Ray AB is the incident light. The rays starting at points F and G and continuing into the substrate are eventually absorbed. Rays BC and DE are components of the overall reflected beam. At point B, the light reflects and refracts. The reflected portion becomes part of the overall reflected beam, and the refracted portion travels through the dark gray layer, and reflects and refracts again at point F. The refracted portion enters the light gray layer and travels through until it is absorbed. The reflected portion travels back through the dark gray material and reaches point D, where it once again reflects and refracts. The refracted portion joins the overall reflected beam. The reflected portion goes back into the dark gray material where it continues reflecting and refracting according to the above pattern until all of the light has either been absorbed by one of the layers or joined the overall reflected beam leaving the surface. Only a few reflections and refractions are shown in the figure for clarity. The overall reflected beam is made up of individual components that have traveled through the layers varying numbers of times, and each component has different properties (intensity and phase) based on their journeys. These beams produce interference with each other, resulting in a distinct polarization that can be analyzed to determine the sample properties [25].

As light travels through different materials, its frequency stays constant. Because the speed of the light changes, but the frequency is remains constant, the wavelength of the light changes, thus changing the phase of the overall reflected beam [25]. Speed, wavelength, and frequency are

related by Equation 7, where v is the speed of the light in the material, f is the frequency, and λ is the wavelength.

$$v = f\lambda \tag{7}$$

Ellipsometry can only be used to measure the thickness of thin films. In this context, "thin" has a very specific meaning that is unique to each material. In order for a film to be measureable by ellipsometry, a portion of the light that enters the film must reach the interface between the lowest film layer and the substrate, be reflected, and reach the ambient again to be collected by the detector [25]. If no portion of the light travels completely through the sample and back to the ambient, then the information about the thickness of the film cannot be obtained, as it has been lost with the light. This exact thickness is dependent on the material's coefficient of extinction.

The Fresnel Relations are used to track the light's polarization change throughout its interaction with the sample [25]. These equations can be extended for any number of sample layers, or reduced to only one as needed to match the situation. The equations presented below are generalized for a sample that has N layers.

$$N_i = n_i - jk_i \tag{8}$$

$$r_{ij}{}^{P} = \frac{N_j \cos\varphi_i - N_i \cos\varphi_j}{N_j \cos\varphi_i + N_i \cos\varphi_j} \tag{9}$$

$$r_{ij}{}^{S} = \frac{N_i \cos\varphi_i - N_j \cos\varphi_j}{N_i \cos\varphi_i + N_j \cos\varphi_j} \tag{10}$$

$$R^{P,S} = \frac{\sum_{i=1}^{N-2} r_{i,i+1}{}^{P,S} + \sum_{i=N-1}^{N} r_{i,i+1}{}^{P,S} exp(-j2\beta_i)}{1 + \prod_{i=1}^{N-1} r_{i,i+1}{}^{P,S} \exp(-j2\beta_i)} \tag{11}$$

$$\beta_i = 2\pi \left(\frac{t_i}{\lambda_i}\right) N_i \cos\varphi_i \tag{12}$$

Equation 8 defines the complex index of refraction, N, which is a convenient way of representing a material's index of refraction n, and its coefficient of extinction k. This quantity goes into Equations 9 and 10 which are the reflectance coefficients for each individual layer in the sample in the parallel and perpendicular directions to the light's direction of travel. The individual reflectance coefficients are parameters of Equation 11 which is the overall reflectance coefficient for the entire sample. The value β in the overall reflectance coefficient equation is defined by Equation 12. This term tracks the phase change of the light as it moves through the sample's layers. It is important to note that β includes the thickness, t, of the layer, because that will ultimately be the parameter of interest in quantifying thermal stability.

The ellipsometer measures two parameters, Δ and Ψ. Ψ is a ratio of the overall reflectance coefficients defined by Equation 13, and Δ is the phase change between the incoming and outgoing light defined by Equation 14. Ψ, Δ, and the overall reflectance coefficients are related through the fundamental equation of ellipsometry, shown below in Equation 15 [26]. At each measurement location, data is taken over a range of wavelengths, so that the result is an experimental set of Δ

and Ψ versus wavelength. The experimental data will be matched by the optical models detailed in coming sections to determine the deposit thicknesses.

$$\tan \Psi = \frac{|R^P|}{|R^S|} \tag{13}$$

$$\Delta = phase\ of\ incoming\ light - phase\ of\ outgoing\ light \tag{14}$$

$$\tan \Psi e^{i\Delta} = \frac{R^P}{R^S} \tag{15}$$

Equipment

A Horiba spectroscopic ellipsometer (Auto SE) shown in Figure 9 was used to make the ellipsometric measurements presented in this work. The Auto SE has a spectral range of 400 to 1100 nm and 70° angle of incidence. The sample viewer is a CCD camera with a field of view of 1.33 by 1 mm and a resolution of 10 μm [27]. The Auto SE has a stage inside that moves in all three spatial directions to position the sample. There is a specially manufactured tube mount on the stage to hold the sample in place during positioning and data collection.

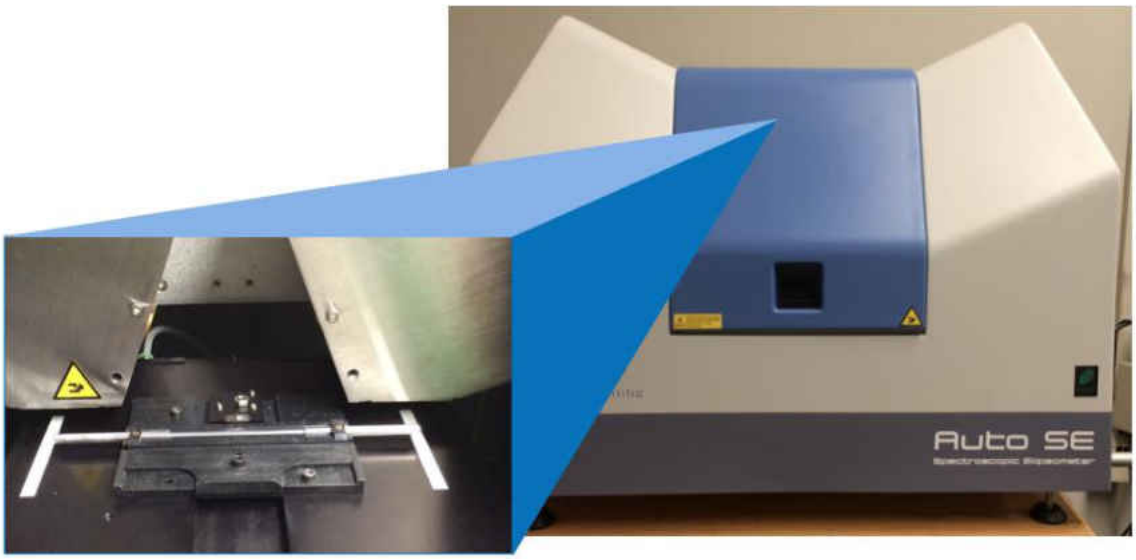

Figure 9: Horiba spectroscopic ellipsometer used in this work

In the most basic sense, an ellipsometer is made up of four optical components: a light source, polarizer, detector, and analyzer [25]. This set up is diagramed in Figure 10. Unpolarized light is produced by the light source and then passes through the polarizer, giving it a linear polarization. The light then encounters the sample and reflects off of it. Because of this interaction, the light is now elliptically polarized. This light is captured by the detector and then analyzed to determine its component properties, which will eventually be used to determine the deposit thickness.

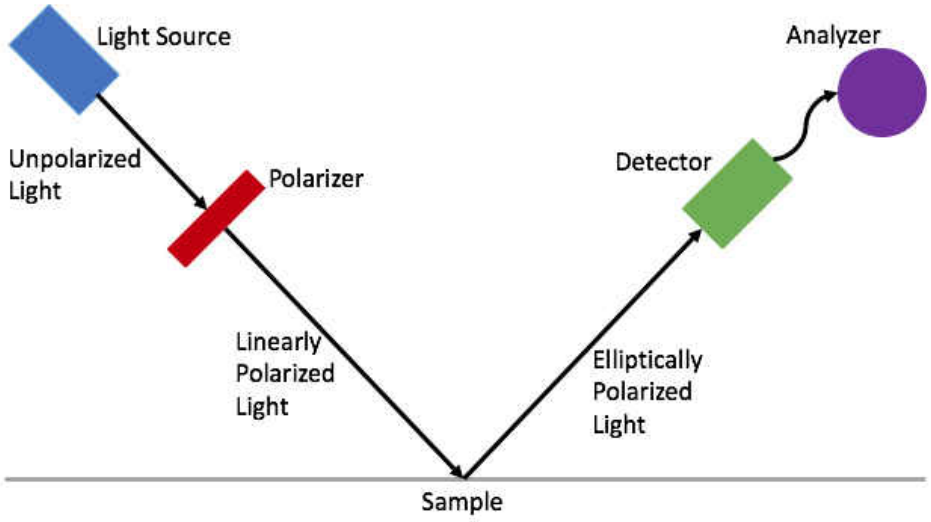

Figure 10: Basic components of an ellipsometer

The tubes are exposed to the fuel using an Alcor Hot Liquid Process Simulator, model HLPS-400. The HLPS is specifically made to conform to the requirements of the ASTM D3241[5] standard for testing aviation fuel thermal stability [28]. The tube is held in a shell, which the fuel flows into and over the tube. The tube is resistively heated to the test temperature, and the fuel is flowed over it at a specified rate for 2.5 hours. Then, the tube is allowed to cool, and it is removed from the HLPS. At this point, various tests for thermal stability can be performed, including the color test and measurements using an ellipsometer. A schematic of the HLPS is shown in Figure 11. The fuel starts in the fuel reservoir, then travels through the inlet line to the test section, where it enters the shell and flows over the tube. Because the tube is heated, the fuel heats as it passes over the tube. Deposits can then form on the tube surface. The fuel exits the test section through the outlet line, then flows through the metering pump which controls the flow rate. The fuel then travels back to the reservoir through the return line.

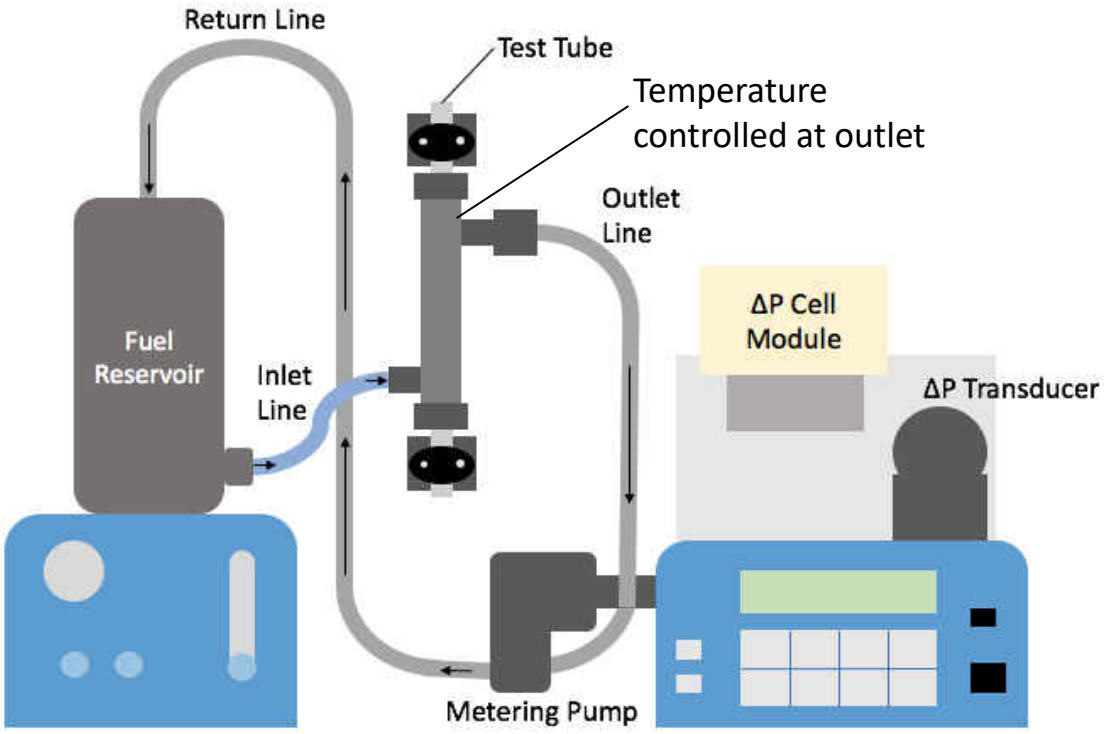

Figure 11: Schematic of the Hot Liquid Process Simulator

An ellipsometric measurement session starts with calibrating the ellipsometer. This is done using an aluminum reference sample built in to the ellipsometer stage. Calibration was performed at least once per week, or whenever the ellipsometer was turned off and on. Next, the tube is put into the sample holder on the stage inside the ellipsometer and secured. The circumferential positioning of the tube is done using the serial number on the right side of the tube. The number is positioned facing up or down depending on the profile location. Data points are taken every 2 mm along the tube's length between -28 and +28 mm along the length of the tube with 0 mm being located at the midpoint. The stage with the sample on it must be positioned for correct alignment with the optical components. First, the x location is input as 28. Then, the y and z positions are

tuned to get the sample inside the viewing area of the camera. Spot 5, which is 70 μm in width by 250 μm in length, was used for data collection because it is large enough to allow enough light to be collected by the detector, but small enough to achieve adequate resolution. The longer dimension of the spot was oriented along the length of the tube to minimize curvature effects from the surface. In cases where a sample was too dark for spot 5 to be usable, spot 6 (250 by 250 μm) or 7 (250 by 500 μm) was used. A 30 second data acquisition routine was used. Once the data point at 28 mm was taken, the rest of the points from 26 to -28 were taken in the same manner. This process was repeated for each tube.

Optical Models

Various theoretical optical models were used to match the experimental results measured by the ellipsometer, and ultimately to determine the film thickness of the deposits left by the jet fuel on the test tube. The goal of the modeling process is to find a way to represent how the optical constants, the index of refraction and coefficient of extinction, change with wavelength. Reference materials were sometimes used for the substrate layer and its oxide if one was present. Reference materials are tables of n and k values at discrete wavelengths. These values cannot be varied during the fitting process, which leads to a typically inflexible model. However, this representation strategy works well for materials that have been thoroughly studied. The other option for material representation is using a dispersion formula. Dispersion formulas are sets of equations that define a particular shape for the n and k curves with wavelength. These equations show how the optical constants change with wavelength over a continuous range, which is different from the discrete

points provided by the reference material models. The parameters of these equations can be varied during the fitting process to affect the fit of the model.

The new amorphous dispersion was investigated in this work because it typically models hydrocarbons well, and conforms to the published values for the optical constants of carbon films from ASTM standards. The important defining quantities of the equations of the new amorphous dispersion [29] are f_j, ω_g, Γ_j, and n_∞. These parameters are important to understand because they can be tuned to affect the fit of the model with the experimental results. The parameter f_j is proportional to the height of the j^{th} peak of the k curve, ω_g is the photon energy at which the k curve is first nonzero, ω_i is the photon energy location of the peak, Γ_j is proportional to the full width at half maximum of the peak in the k curve, and n_∞ is the value of the n curve as the photon energy of the incident light approaches infinity.

$$k(\omega) = \sum_{j=1}^{N} \frac{f_j(\omega - \omega_g)^2}{(\omega - \omega_j)^2 + \Gamma_j^2} \; for \; \omega > \omega_g \tag{16}$$

$$k(\omega) = 0 \; for \; \omega \leq \omega_g \tag{17}$$

$$n(\omega) = n_\infty + \sum_{j=1}^{N} \frac{B_j(\omega - \omega_j) + C_j}{(\omega - \omega_j)^2 + \Gamma_j^2} \tag{18}$$

$$B_j = \frac{f_j}{\Gamma_j}\left[\Gamma_j^2 - (\omega_j - \omega_g)^2\right] \tag{19}$$

$$C_j = 2 f_j \Gamma_j (\omega_j - \omega_g) \tag{20}$$

The generalized equations are shown here for optical constant curves that have any number of peaks in them. These equations are functions of ω, or the photon energy of the incident light. This can be easily converted to the light's wavelength, which may be more intuitive to understand, however the equations are cleaner if the photon energy of the light is considered. Energy in electron volts and wavelength in μm are related through h (Planck's constant) and c (the speed of light in a vacuum) as shown in Equation 21.

$$E = \frac{hc}{\lambda} \tag{21}$$

The typical shape of a new amorphous dispersion is shown in Figure 12. In some instances, roughness layers were also added to the models. A roughness layer is represented by a mixture of the material of the layer underneath the roughness and a void, typically in a 50-50 blend ratio. The void represents the empty space in the top material layer caused by the peaks and valleys in the material surface. The roughness layer has the optical properties of a blend of the two materials.

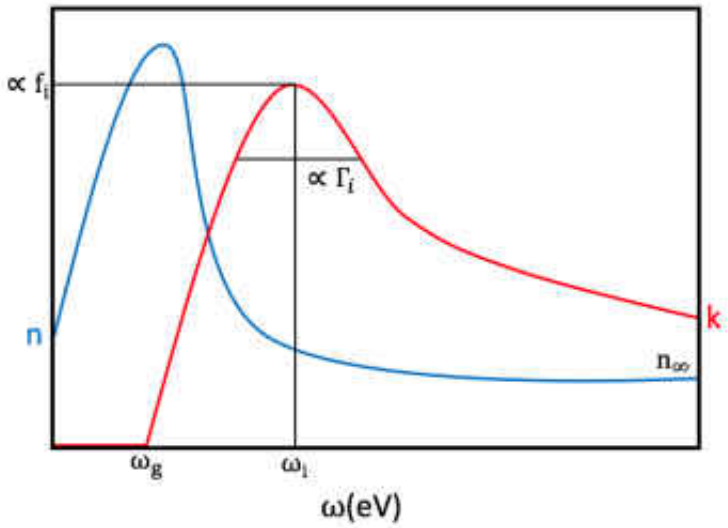

Figure 12: New amorphous dispersion formula

The Tauc-Lorentz dispersion was also investigated in this work. This dispersion describes a shape shown in Figure 13. The equations which govern this dispersion are given by Equation 22 through 29 [30].

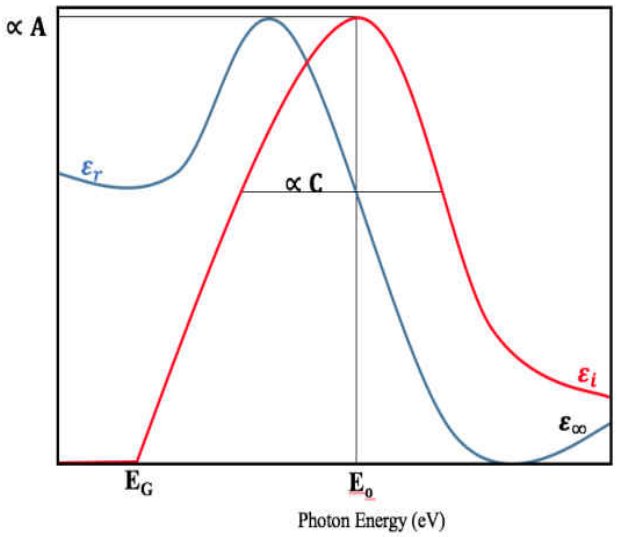

Figure 13: Tauc-Lorentz dispersion formula shape

The Tauc-Lorentz dispersion defines the optical constants by the dielectric function, ε, which is equal to the complex index of refraction squared. This is just a different bookkeeping strategy for recording the optical constants. This dispersion is also in terms of photon energy, like the new amorphous dispersion.

The important parameters in these equations are E_0, which is the location of the peak of the ε_i curve, E_g which is the first energy at which ε_i is non-zero, C, which is proportional to the full width at half maximum of the peak, A which is proportional to the peak height, and $\varepsilon_\infty$is the value of the ε_r curve as the energy of the incoming light approaches infinity. These parameters are similar to those in the new amorphous dispersion formulas, but are used differently in the equations shown below.

$$\varepsilon_{i,TL}(E) = \frac{1}{E}\frac{AE_0C\left(E - E_g\right)^2}{\left(E^2 - {E_0}^2\right)^2 + C^2E^2} \; for \; E > E_g \tag{22}$$

$$\varepsilon_{i,TL}(E) = 0 \; for \; E \leq E_g \tag{23}$$

$$\varepsilon_{r,TL}(E) = \varepsilon_\infty + \frac{AC a_{ln}}{2\pi\zeta^4 \alpha E_0} ln\left[\frac{{E_0}^2 + {E_g}^2 + \alpha E_g}{{E_0}^2 + {E_g}^2 - \alpha E_g}\right]$$

$$-\frac{A}{\pi}\frac{a_{atan}}{\zeta^4}\left[\pi - \arctan\left(\frac{2E_g + \alpha}{C}\right) + \cdots + arctan\left(\frac{\alpha - 2E_g}{C}\right)\right]$$

$$+\frac{4AE_0E_g(E^2 - \gamma^2)}{\pi\zeta^4\alpha} X \ldots X \left[arctan\left(\frac{\alpha + 2E_g}{C}\right) + \arctan\left(\frac{\alpha - 2E_g}{C}\right)\right]$$

$$-\frac{AE_0C}{\pi\zeta^4} E_g ln\left[\frac{|E - E_g|(E + E_g)}{\sqrt{\left({E_0}^2 - {E_g}^2\right)^2 + {E_g}^2 C^2}}\right]$$

(24)
$$a_{ln} = \left({E_g}^2 - {E_0}^2\right)E^2 + {E_g}^2C^2 - {E_0}^2\left({E_0}^2 + 3{E_g}^2\right)$$

(25)
$$a_{ln} = \left(E^2 - {E_0}^2\right)\left({E_0}^2 + {E_g}^2\right) + {E_g}^2C^2$$

(26)
$$\alpha = \sqrt{4{E_0}^2 - C^2}$$

(27)
$$\gamma = \sqrt{\frac{{E_0}^2 - C^2}{2}}$$

(28)
$$\zeta^4 = (E^2 - \gamma^2)^2 + \frac{\alpha^2C^2}{4}$$

(29)

The modeling and fitting process is automated by a program called DeltaPsi2 [31] which was developed by Horiba, the manufacturer of the ellipsometer used in this study. The models look

similar to Figure 14 which shows a purple layer for the substrate and a blue layer on the top for the deposit.

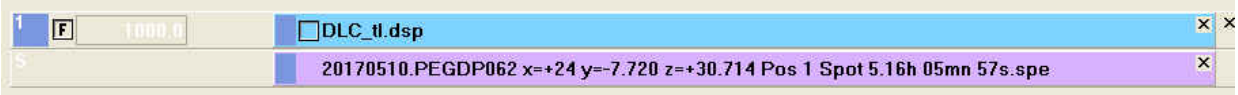

Figure 14: Typical model representation in DeltaPsi2

To start, a thickness value for each of the layers in the model is guessed. This thickness and the optical representation chosen are used to generate theoretical n and k curves. These then become inputs for the Fresnel Relations and the fundamental equations of ellipsometry to obtain theoretical Δ and ψ curves versus wavelength. These theoretical curves are compared to the experimentally obtained ones from the ellipsometer over the same wavelength range. χ^2 is a statistical metric that is used to quantify the goodness of fit between the two, with lower χ^2 values indicating closer agreement between the model and experimental data. The fit parameters (generally the thickness and defining parameters of the optical model) are iterated until a minimum χ^2 is achieved. χ^2 is an important metric for assessing the quality of the fit of the model, however it was found that models that yielded χ^2 on the order of 0.1 were trying to fit the noise in the data, resulting in nonphysical thickness profiles. χ^2 values on the order of 10 generally produced better results.

Thickness profiles were analyzed primarily by identifying the maximum deposit thickness. This is the parameter required for determining a fuel's thermal stability by ASTM D3241[5]. A maximum thickness of less than or equal to 85 nm is considered passing the ellipsometric test for thermal stability. In addition, total deposit volumes were calculated by taking the area under the

thickness profile through numerical integration with Riemann sums and multiplying by the circumference of the tube. This assumes that the thickness profile is constant around the tube circumference, however measurements made at other circumferential locations suggest that this is approximately accurate.

The Tauc-Lorentz dispersion was ultimately chosen to model all of the results presented here. This choice will be explained in the validation section.

CHAPTER FOUR: FINDINGS

A typical result is shown in Figure 15 below. The blue vertical lines indicate the starting and ending points of the profile, as well as a point at which the deposit thickness and tube discoloration change significantly. The tube can be seen in the top part of this graphic, and the deposit is visible as the darker section on the right side. Data is taken along the thinner middle section of the tube, which is the part exposed to the fuel. The larger end sections, often called shoulders, are for holding the tube in place. The darker part of the deposit corresponds to the thicker part of the profile; however, it is interesting to note that there is a level of deposition along the entire length of the tube as shown by the thickness profile, which is not visible to the eye. This highlights the benefits of using the ellipsometer to measure the thickness profile, rather than using the color standard which relies on the abilities of the human eye. A much higher level of detail is discernable with the ellipsometer that is not immediately visible, as indicated by the thickness profile.

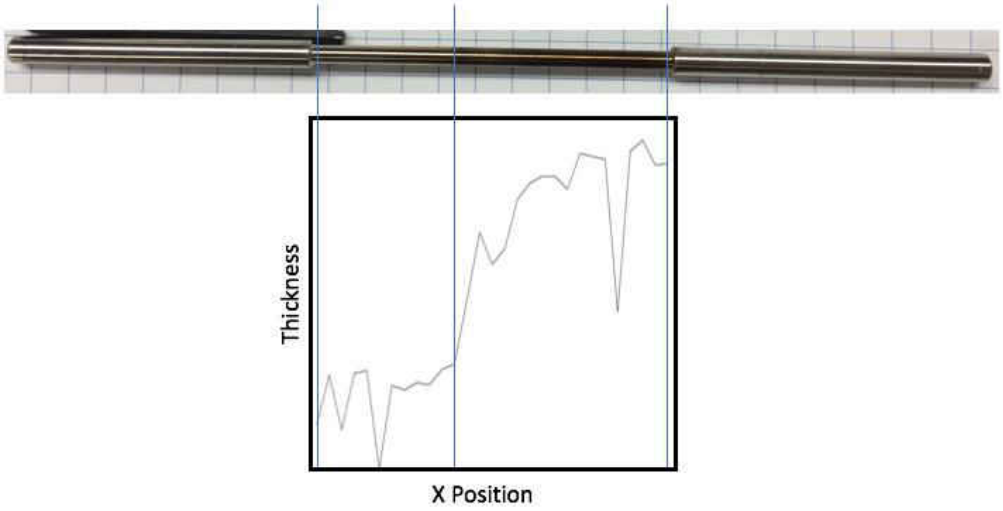

Figure 15: Qualitative comparison between tube discoloration and thickness profile

The characteristics of the deposit profile shown in the figure are representative of the thickness profiles obtained for each tube studied within this work. The deposition level along the tube changes proportionally to the temperature profile along the tube. The temperature of the tube is controlled using a thermocouple located approximately 20 mm to the left of the tube's right shoulder, at the test section exit of the HLPS. The temperature is known at this point, and the voltage across the tube is changed accordingly to achieve the desired test temperature. The temperature along the rest of the tube varies, as it is not being monitored directly at those points. It is expected that from right to left along the tube, the thickness profile rises from its initial level to a peak somewhere near the thermocouple location, then decreases towards the end of the tube (which is located near the start of the test section).

Two circumferential, or angular positions were analyzed on each tube. The first, identified as Position 1, is in line with the serial number printed on the left-hand tube shoulder. All tubes were oriented in the ellipsometer with the serial number on the left. The second position, termed Position 3, is located on the opposite side of the tube, 180° from Position 1. In most cases, there was fairly good agreement between the thickness profiles at both positions.

Aluminum Oxidation Study

Studies of the aluminum oxide on clean tubes were performed in order to assess the level of oxidation present on the tubes before they were exposed to the fuel. This was necessary to create a realistic substrate to model the other samples. Ideally, the same tube would have been analyzed using the ellipsometer both before and after exposure to the fuel, and the data points from the pre-

exposure analysis would have been used for the substrate for modelling that tube. This would have produced the most accurate models and accounted for the specific surface irregularities of each location. Unfortunately, this was not possible because the samples were created prior to the start of this work, so the method detailed here was deemed to be the next most accurate. Several clean tubes were analyzed using the ellipsometer and modeled using aluminum and aluminum oxide reference materials. This was a simple model, containing only the substrate and the oxide layer. These tubes had never been exposed to any fuel, so it was assumed that anything on the base aluminum layer was oxide, and nothing else. These tubes were also stored in the same conditions as the tubes that were exposed to the fuel, so it can be assumed that both sets would have similar levels of oxidation. Data points from along the lengths of each tube were analyzed. The oxide layers measured between 10.42 and 15.84 nm in thickness, with an average of 12.11 nm. The data point with the oxide layer thickness closest to the mean was chosen as the substrate in the model used to analyze all of the tubes exposed to fuels. This point had an oxide layer thickness of 11.58 nm. Statistical analysis of all of the clean data points indicates that this oxide layer thickness can be assumed to be accurate for the entire population within ±0.3 nm at a 95 percent confidence interval. Figure 16 shows the oxide layer profile of one of these clean tubes. This demonstrates how the oxide layer does not change significantly over the length of the tube, and the substrate chosen is expected to closely match the oxide layer of most points on all of the tubes.

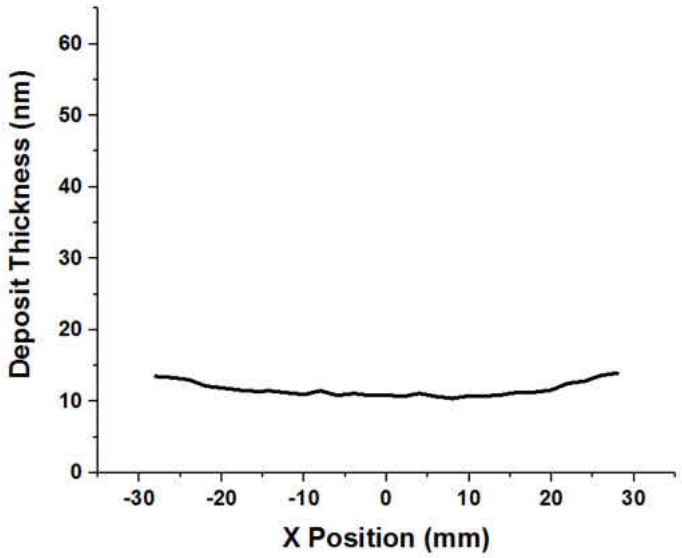

Figure 16: Aluminum oxide layer thickness for a typical clean aluminum tube

The use of this substrate in the model for the tubes exposed to the fuels means that a layer of oxide is accounted for within the substrate, without having to add an extra layer to the model. This was found through the reference tubes to be the most accurate modeling method, rather than trying to use a three-layer model (a model with a substrate, oxide layer, and carbon film layer on the top). Ideally, data would have been taken on the clean aluminum tubes and then those same tubes would have been exposed to the fuel so that each point could have had its own individualized substrate accounting for the exact aluminum oxide layer thickness at every point on each tube. This would have been very computationally time consuming because each data point on each tube would have had a different model, and this would have prevented the use of automated batch modeling, but this method would have yielded the most accurate results. However, it is likely that the chosen substrate is close to the actual conditions at each point, so it is estimated that this contributes only a small amount to the uncertainty in the measurements. Additionally, this could

not have been done because the tubes were exposed to the fuels prior to the start of this work, but this should be considered for future studies.

Sasol IPK Aluminum Tubes

Aluminum tubes exposed to Sasol IPK with varying levels of naphthalene were analyzed over a fuel temperature range of 300 to 380 °C. The raw data is summarized in Appendix A. All of the tubes achieved a passing rating on the JFTOT color test of 1 or <2. They all also achieved passing ratings using the ellipsometry thickness standard. Maximum deposit thicknesses as well as well as total deposit volumes are presented.

As the temperature of the fuel increases, the maximum deposit thickness is expected to also increase. This is because at higher temperatures, more of the reactions breaking down the fuel would be occurring, and they would be occurring more rapidly, leading to increased deposit levels. Tubes 1304, 1305, 1306, and 1335 span a fuel temperature range from 300 to 380 °C, all with 0 percent naphthalene. The maximum thicknesses and the deposit volumes for these tubes do not follow the expected monotonically increasing trend. This could be due to irregularities in the metal tube surface, and this fact highlights the importance of measuring the tube surface profile using the ellipsometer prior to exposing the tube to the fuel. Tubes 1344, 1330, and 1327 over a test temperature range of 340 to 380 °C with 3 percent naphthalene also do not show this trend. Between the lowest and highest temperature the deposit thickness and volume do indicate increases in this case. Interestingly both sets show deposit peaks (in maximum thickness and deposit volume) at similar temperatures (345 and 360 °C respectively). Further investigation is necessary to understand the mechanism breaking down the fuel in this temperature range contributing to the

deposit peak, but this result suggests that the mechanism breaking down the fuel is not as simple as was expected at the outset of this work. Figure 17 and Figure 18 show the trends of increasing temperature at constant fuel composition on aluminum tubes for the 0 and 3 percent naphthalene cases.

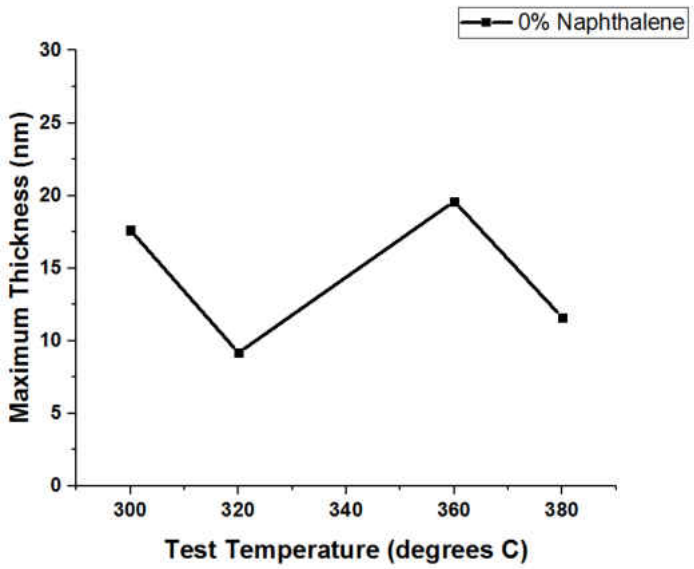

Figure 17: Maximum deposit thickness versus test temperature for pure Sasol IPK and aluminum tubes

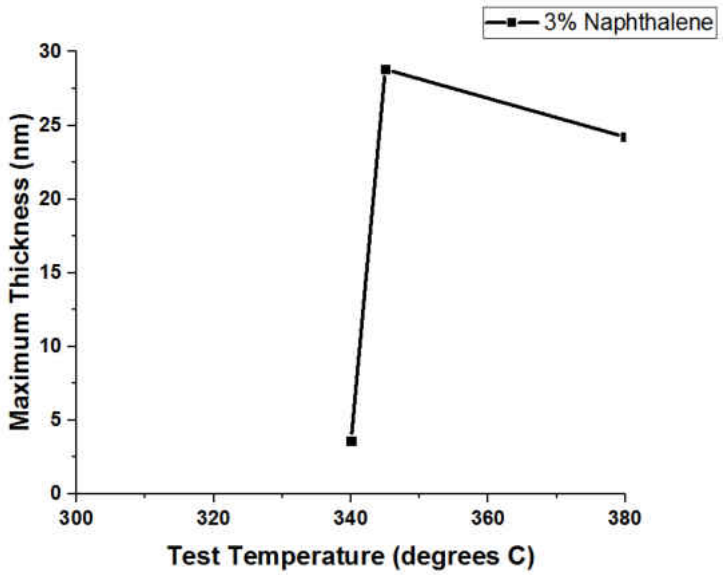

Figure 18: Maximum deposit thickness versus test temperature for 3 percent naphthalene in Sasol IPK and aluminum tubes

Tubes 1321 and 1322 were tested at the same fuel temperature, 300 °C, and with the same naphthalene concentration, 5 percent, however the maximum thicknesses and total deposit volumes for these samples are quite different with a more than 100 percent difference in maximum thickness, and more than 50 percent difference in volume. It is possible that these differences may be attributable to surface irregularities in the substrates and not the deposits themselves, but it is not possible to know this without measuring the surface profile of the tube before exposing it to the fuel. It is also interesting to note that the maximum deposit thicknesses and deposit volumes do not change in the same proportion here, suggesting that the maximum thickness is not a reliable method for determining how much deposit is present. Tubes 1337 and 1310 were also tested with identical conditions (380 °C and 1 percent naphthalene). The maximum thicknesses show much closer agreement in this case (21.41 and 29.14 nm respectively). It is however, interesting to note the differences in total deposit volume between these two samples. This indicates that while the

two had similar peak thicknesses, one profile was thicker on average to produce the greater volume. Reporting only the maximum thickness as is required by ASTM D3241 may not provide adequate representation of a fuel's thermal stability. Figure 19 and Figure 20 show two representative thickness profiles for these measurements.

Tubes 1304, 1321, and 1322 were all tested at a fuel temperature of 300 °C with varying naphthalene concentration from 0 to 5 percent. Tubes 1321 and 1322 are repeated verifications as noted above, however it is difficult to make comments about the effect of the naphthalene because depending on which 5 percent tube is chosen, opposite trends are seen. In the case of tubes 1335 and 1337 at 380 °C and 0 and 1 percent naphthalene respectively, as the concentration of naphthalene increases, the maximum deposit thickness increases dramatically. However, if the total deposit volume is examined, it is found that the total deposit increases minimally with the increased naphthalene. This again highlights the fact that maximum thickness does not provide a complete picture of the fuel's behavior, and that both deposit volume and maximum thickness should be considered. It must be emphasized here that all of the abovementioned comparisons would have been impossible to make with only data obtained from the color standard (as in the traditional JFTOT).

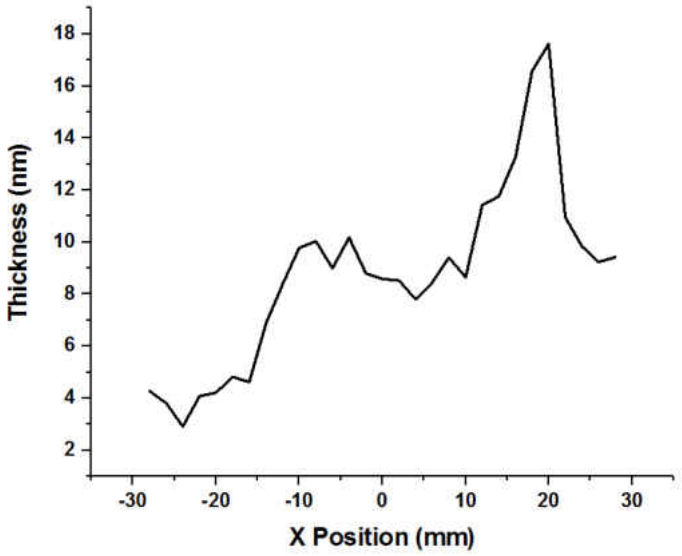

Figure 19: Thickness deposit profile for aluminum tube 1304 exposed to Sasol IPK with 0 percent naphthalene at 300 °C

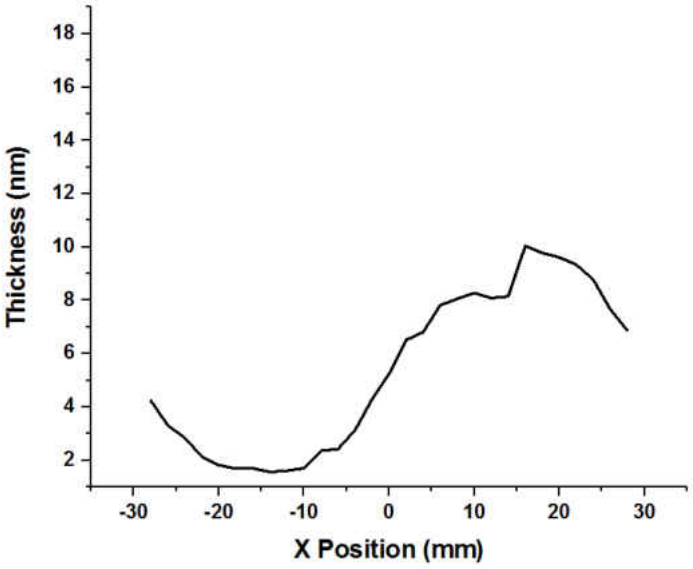

Figure 20: Thickness deposit profile for aluminum tube 1321 exposed to Sasol IPK with 5 percent naphthalene

Sasol IPK Stainless Steel Tubes

Stainless steel tube substrates were exposed to Sasol IPK over a temperature range of 385 to 400 °C with 0 to 5 percent naphthalene by volume. The results are summarized in Appendix A. All of these tubes failed the color test for thermal stability. Additionally, all of these tubes resulted in maximum thicknesses that would rate them as thermally unstable (>85nm). It is not surprising that the stainless steel tubes all failed the color test because the color standard is only applicable to aluminum tubes. It is however, worth analyzing these tubes further, because as was seen with the aluminum tubes above, subtle differences are present that are not immediately noticeable.

The deposit amount is also expected to increase with temperature for the stainless steel cases (as was expected for the aluminum cases above). Tubes 1309 and 1308 agree with this hypothesis in maximum deposit thickness. Tubes 1311, 1329 were tested at fuel conditions of 385 °C and 1 percent naphthalene. Tube 1328 was also exposed to 1 percent naphthalene, but at 400 °C. Between tubes 1311 and 1328 the deposit thickness increases, however between tubes 1329 and 1328 it decreases with the increase in temperature. In this case it is instructive to consider the deposit volumes. The volumes for the two tubes at 385 °C are similar (0.0197 mm^3 and 0.0194 mm^3 respectively), as would be expected for identical test conditions. The volume for the tube at 400 °C increases to 0.0222 mm^3. This also agrees with the initial hypothesis. This highlights the need to examine not only the peak deposit thickness but the total deposit volume as well.

Considering tubes 1309, 1308, 1311, and 1328 the increase in maximum deposit thickness is greater for the 0 percent naphthalene tubes, however the range here is also larger. If the increase in thickness is assumed to be linear, then for an equal increase in temperature the deposit thickness with 1 percent naphthalene increases more. It should be noted that this linearization is only an

approximation, but in the absence of other data on this fuel it is an acceptable assumption to make.

Figure 21 and Figure 22 show representative thickness profiles for the stainless steel cases.

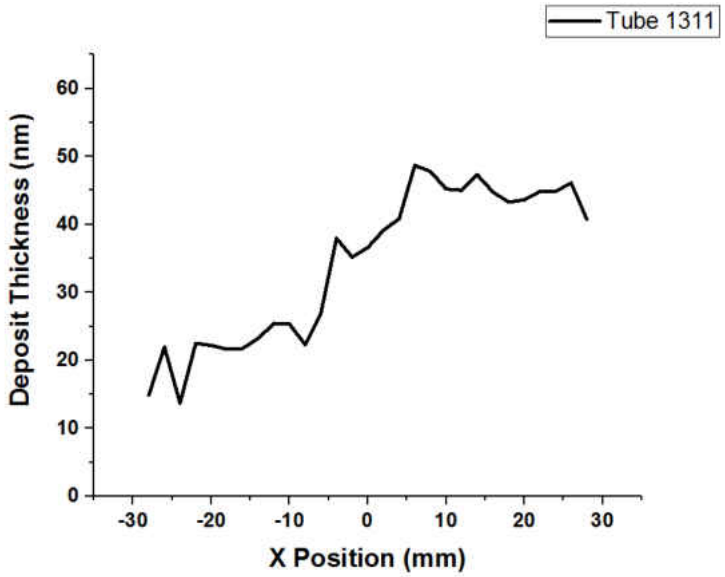

Figure 21: Deposit thickness profile for stainless steel tube 1311 exposed to Sasol IPK with 1 percent naphthalene at 385 °C

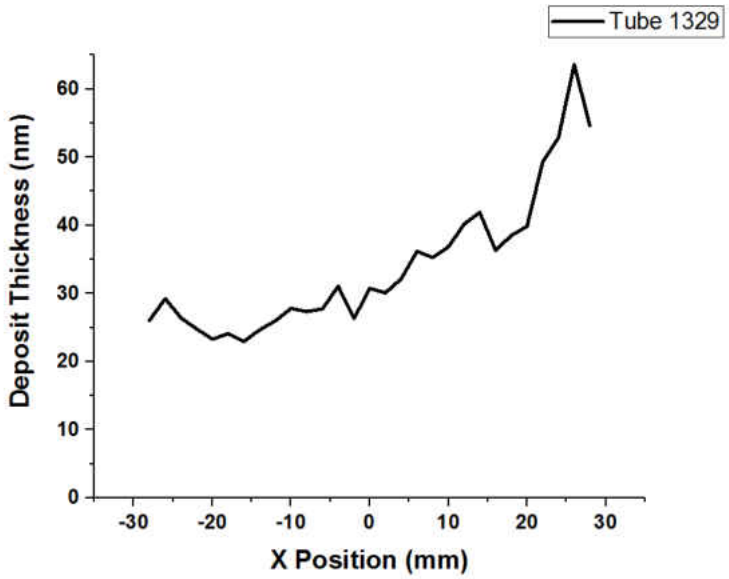

Figure 22: Deposit thickness profile for stainless steel tube 1328 exposed to Sasol IPK with 1 percent naphthalene at 400 °C

Tubes 1311 and 1329 were tested at a fuel temperature of 385 °C and 1 percent naphthalene. These tubes yielded maximum thicknesses of 48.43 and 63.60, respectively. Some of this difference could be caused by surface differences in the steel substrate. Here, it is again useful to look at the total deposit volumes which are 0.0197 and 0.0194 mm^3 suggesting an acceptable level of repeatability in the deposit volume measurement. This also indicates the sensitivity of the peak deposit thickness to some unknown factor that the deposit volume is not sensitive to. This may make the deposit volume a more useful measure of thermal stability.

Tubes 1309, 1311, 1329, 1332, and 1333 were all tested at 385 °C. The test fuels for these tubes are Sasol IPK with naphthalene ranging from 0 to 5 percent by volume. As the naphthalene concentration increases the maximum thickness does not show a clear trend. The deposit volume on the other hand increases as the concentration of naphthalene increases, which is shown

graphically in Figure 23. This indicates that the naphthalene is having a negative impact on the thermal stability of the Sasol IPK.

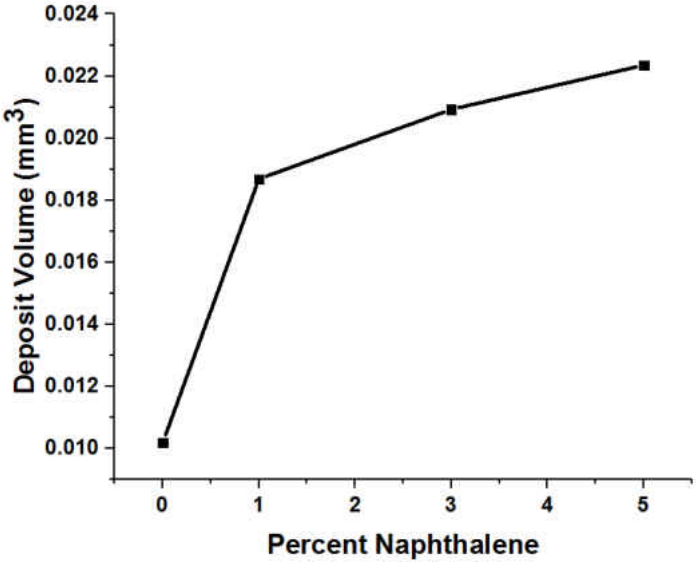

Figure 23: Deposit volume versus percent naphthalene on stainless steel tubes

Gevo Tubes

First, the effect of increasing temperature on pure Gevo was examined, and the results of these tests are summarized in Figure 24. The raw data for all Gevo samples is contained in Appendix B. Data sets for two circumferential locations are shown here and defined as follows: Position 1 is in line with the serial number on the tube, and Position 3 is located 180° away, on the opposite side of the tube. While there are minimal differences between the two positions, the same trends exist for both. In this case, the same trends are also seen in the calculated deposit volumes.

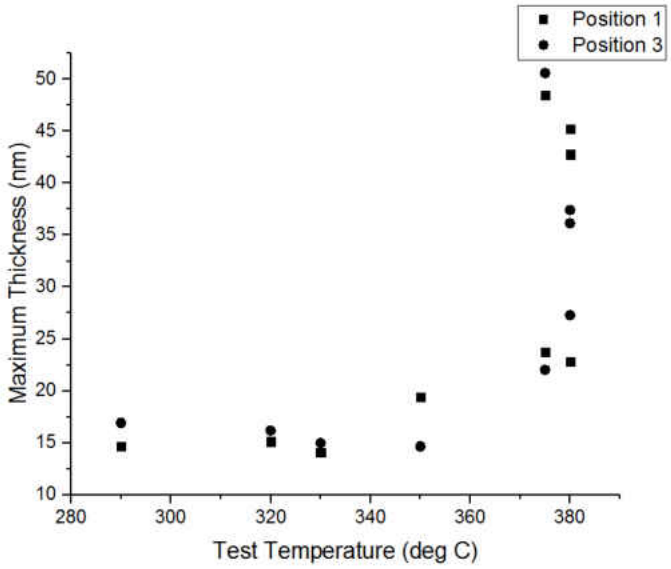

Figure 24: Maximum deposit thickness versus temperature for Gevo fuel on aluminum tubes

The maximum deposit height is relatively constant until the temperature reaches approximately 375 °C, at which point it increases exponentially. It should be noted that none of these tubes has a maximum deposit thickness of more than 85 nm, so the thermal breakpoint temperature has not yet been reached. By extrapolating from this data, it can be assumed that the breakpoint would be reached within 25 to 50 °C, given the drastic increase in deposit height measured at the higher temperatures.

For comparison, a similar analysis was performed on pure JP-8 fuel, and the raw data for these tests is given in Appendix C. JP-8 is a traditional kerosene based fuel commonly used by the United States military. The results are shown in Figure 25 and exhibit similar trends to the Gevo fuel. In this case, the deposit thickness begins increasing at approximately 300 °C, which is lower than that of the Gevo, and this batch reaches a higher level of deposition more quickly. This batch has also not yet reached its thermal breakpoint temperature because none of the samples show maximum deposit thicknesses greater than or equal to 85 nm, but it can also be assumed that the

thermal breakpoint would be shortly reached. These results indicate that the JP-8 is less thermally stable than the Gevo. This is as would be expected because the Gevo fuel contains lower levels of aromatics, which are known to negatively impact thermal stability.

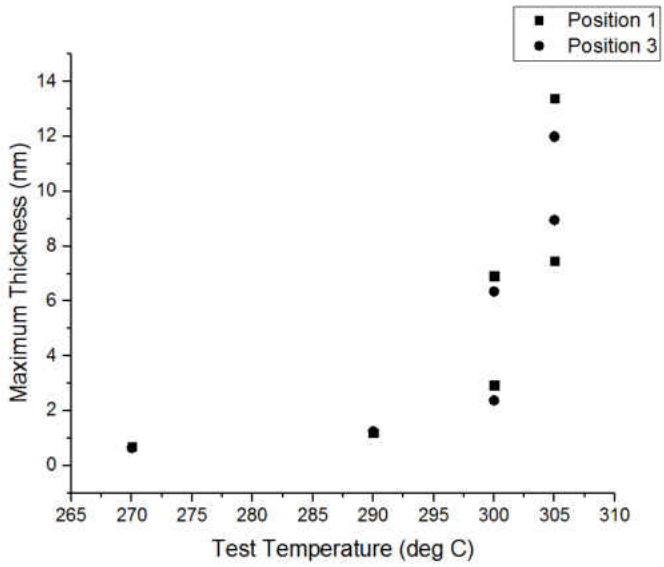

Figure 25: Maximum deposit thickness versus temperature for JP-8 on aluminum tubes

The effect of increasing temperature on a blend of 85 percent Gevo with 15 percent JP-8 was investigated. The maximum deposit thickness is relatively constant with increasing temperature, as shown by Figure 26, however there is an exception to this in the point at 350 °C. It is likely that this point is an outlier given that all of the other points lie more or less on a straight line.

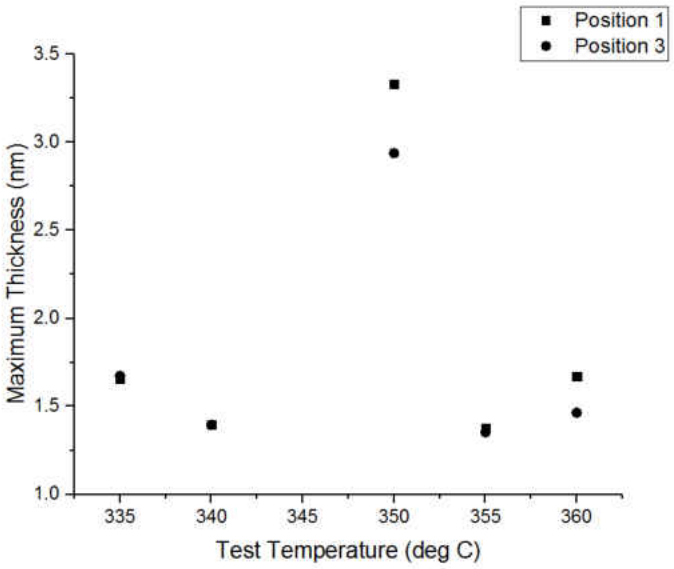

Figure 26: Deposit thickness versus test temperature for 85-15 blend of Gevo and JP-8

The thermal breakpoint is not reached by any of these samples. The region shown here is probably still in the constant deposit maximum region described for the two fuels shown above. If this is true, the blend of Gevo and JP-8 would be more thermally stable than the JP-8, which makes sense given that the pure Gevo fuel was more thermally stable.

The Gevo and JP-8 samples provide an interesting opportunity to examine the color standard rating system. A summary of the color rating and maximum deposit thickness measured for each tube is given in Table 3. For the most part, the maximum thicknesses increase with increasing color rating, and the color rating increases with increasing test temperature. This indicates that thicker deposits are generally darker in color than thinner ones. However, there are instances where the two rating systems disagree. Tube 1243 for instance, fails the color standard test with a rating of <4, but passes the ellipsometric test with a maximum thickness of 74.62. Tubes 1274 and 1275 also fall into this category of failing the color test but passing the ellipsometric test. These two tubes in fact have quite low maximum deposit thicknesses, highlighting how the color

test can be misleading and inaccurate. It is likely that the Gevo deposits do not follow the same color trends as traditional fuels, making the color standard incapable of rating them accurately. The tubes receiving <4 ratings span a deposit thickness range of 13.059 to 134.034 nm, demonstrating how the color standard groups tubes together that are much more different than they are alike. This emphasizes the need for a more detailed test, such as ellipsometry.

Table 3: Gevo Color Rating Comparisons

Tube ID	Fuel	Test Temp	Composition	Color Rating	Max Thick (nm)
1229	N81 GEVO	290	100	2 (pass)	5.048 (pass)
1230	N81 GEVO	320	100	2 (pass)	5.451 (pass)
1231	N81 GEVO	330	100	1 (pass)	4.559 (pass)
1234	N81 GEVO	350	100	1 (pass)	8.593 (pass)
1235	N81 GEVO	375	100	<2 (pass)	34.703 (pass)
1238	N81 GEVO	380	100	<2 (pass)	28.958 (pass)
1257	N81 GEVO	380	100	<2 (pass)	21.069 (pass)
1260	N81 GEVO	375	100	2 (pass)	11.353 (pass)
1262	N81 GEVO	380	100	1 (pass)	10.651 (pass)
1232	N84 JP8	270	100	0 (pass)	6.948 (pass)
1233	N84 JP8	290	100	1 (pass)	11.880 (pass)
1241	N84 JP8	300	100	2 (pass)	29.330 (pass)
1254	N84 JP8	300	100	<3 (pass)	69.160 (pass)
1243	N84 JP8	305	100	<4 (fail)	74.620 (pass)
1256	N84 JP8	305	100	<4 (fail)	134.034 (fail)
1271	N98 GEVO-JP8	330	75-25	<3(pass)	57.953 (pass)
1272	N98 GEVO-JP8	335	75-25	<4 (fail)	50.388 (pass)
1275	N99 GEVO-JP8	340	80-20	<4 (fail)	13.059 (pass)
1274	N99 GEVO-JP8	345	80-20	<4 (fail)	15.681 (pass)

Batch Differences in Jet A

Finally, 13 aluminum tubes were exposed to various batches of Jet A, a traditional jet fuel, all at 260 °C. The data for these tests is given in Appendix D. Their color ratings range from 1 to

4P, and their maximum thickness measurements range from 13.05 to 169.4 nm. Most of the samples do tend to cluster around the 0 to 20 nm maximum deposit range, but there is a significant spread. These wide ranges highlight the differences that exist among different batches of jet fuel, especially one as complex as Jet-A, which contains thousands of components. Because differences like these occur, it is important to have a quick, reliable, and detailed measure of a fuel's thermal stability that can be implemented for every fuel being used. Ellipsometry fits all of these criteria. This also highlights the need to develop jet fuels with fewer components, such as the alternative fuels tested here. Simpler fuels are more likely to be consistent from batch to batch than ones with more components, leading to more predictable deposition behaviors. Figure 27 shows the variation in the maximum deposit thickness for all of the batches of Jet A.

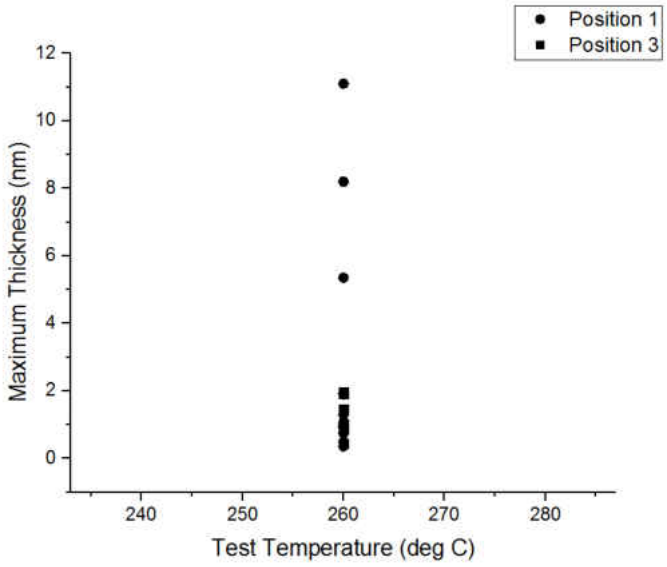

Figure 27: Maximum deposit thickness at 260 °C for various batches of Jet A

Reference Tube Validation

Eight reference tubes were obtained for analysis from Zachary West at Wright Patterson Air Force Base. The researchers at WPAFB had produced aluminum tubes with carbon deposits on them with known thicknesses and had measured the thicknesses with their ellipsometric and interferometric tube raters. Neither measurement had yielded the known thickness value, and additional analysis was desired. This provided an opportunity to validate the models used in determining the deposit thicknesses on the tubes exposed to various fuels because the reference tubes had theoretically known thicknesses.

These reference tubes were created by plasma sputtering a carbon target, and rotating the tube to produce an even distribution around the circumference. Carbon was deposited over approximately 10 mm long sections of each tube. The rest of the surface was covered with Kapton tape during deposition and removed afterwards. The covered sections were cleaned with isopropyl alcohol after the deposition process was finished. This produced plateau-like thickness profiles with well-defined edges on an otherwise clean tube. A typical reference tube thickness profile as measured by the ellipsometer is shown in Figure 28.

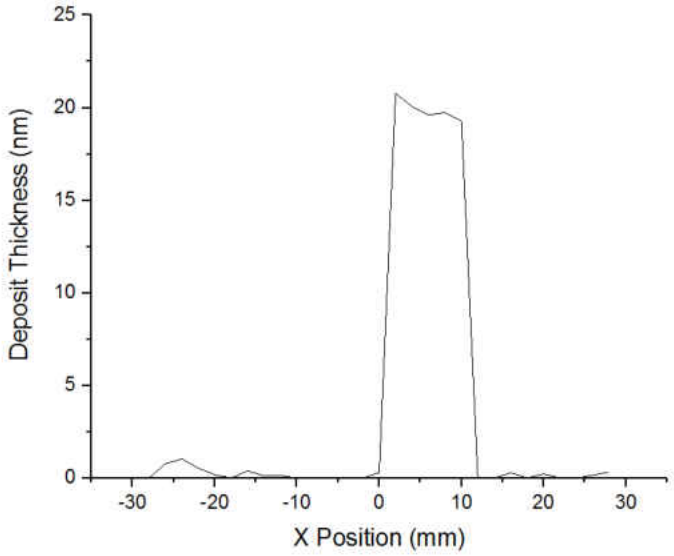

Figure 28: Typical reference tube deposit profile and chi squared values versus x position

The theoretical deposit thicknesses were determined using a deposition rate method. First, a thick carbon film was deposited on a tube over a controlled length of time. This film was thick enough to measure its depth using profilometry. Once the thickness of this relatively larger deposit was known, and the deposition time was also known, a deposition rate in terms of depth per unit time was obtained. Then, tubes with specific thicknesses could be produced by exposing them to the carbon sputtering for a particular length of time. This method makes several assumptions. It assumes that the deposition rate is constant with time, and that it is constant with deposit thickness, meaning that the deposition rate is the same regardless of the thickness of the deposit already present on the tube. It is possible that this rate could be different at the beginning of the process, when the deposit is forming on the clean aluminum surface, than at the middle or end, when it is depositing on an already carbon coated surface, and the implications of this will be discussed in the following paragraphs. This method's accuracy also depends on the accuracy of the timing mechanism and the ability to precisely stop and start deposition at those times.

Because these tubes had theoretically known deposit thicknesses and easy to predict profile shapes, they were used to validate the optical models used to determine the deposit thicknesses on the other tubes exposed to the jet fuels. This provided an opportunity to evaluate the various models and their ability to fit thin carbon films. The composition of the films on the reference tubes were compositionally similar to the ones on the tubes exposed to the jet fuels, and it can be assumed that the models treat them in the same manner. It was found that models that fitted the optical constants of the film along with the deposit thickness tended to lead to profiles that were very jagged, and not at all similar to what would be expected for tubes prepared in the manner described above. However, these models also yielded very low χ^2 values, indicating a close fit between the model and the experimental data. It was determined that models fitting too many parameters were too flexible and thus were fitting the noise in the data, and yielding non-realistic results. Models that only fitted the deposit thickness produced the expected plateau type thickness profile. Various dispersion types were also tried to model these results. New amorphous and Tauc-Lorentz dispersions were investigated, and both were found to give the expected thickness profile shapes, but very different thickness magnitudes. Reference materials for aluminum and aluminum oxide were also tested, and found to yield the appropriate thickness profile shape, but the magnitude of the deposit was always approximately twice the theoretically known thickness value. The Tauc-Lorentz dispersion was found to match most of the reference tubes close to the theoretically known values. Table 4 summarizes these results, and Figure 29 shows a comparison of the thickness profiles that results from the new amorphous, Tauc-Lorentz, and reference material models. These trends were seen for all eight reference tubes.

Table 4: Reference tube results

Tube	Known Thickness (nm)	Average Measured Thickness (nm)	Percent Difference
62	25	19.90	22.73
385	30	27.80	7.60
389	40	39.14	2.18
212	50	50.92	1.83
626	60	70.40	15.96
498	75	73.58	1.92
228	90	61.34	37.87
414	255	224.17	12.87

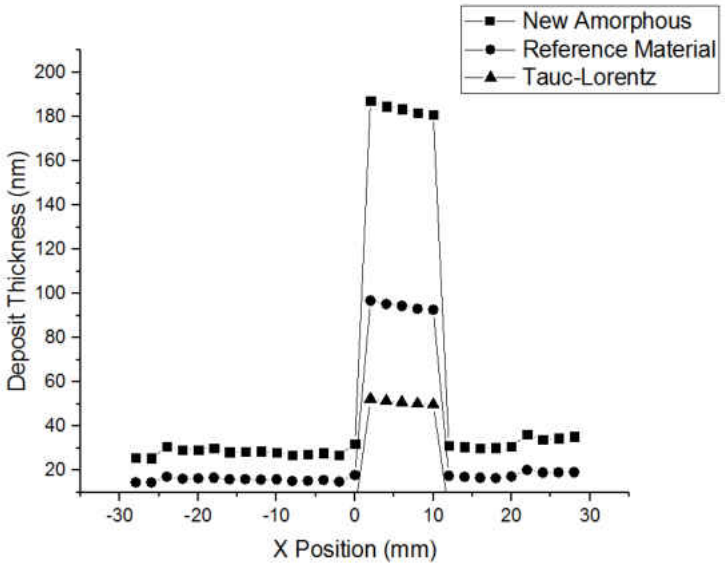

Figure 29: Model comparison for 50 nm reference tube

A few of the tubes were not matched precisely by this model, but it is likely that the assumptions made in calculating the deposition rate were not entirely appropriate in these cases. The 25 nm tube measured 20 nm in thickness. This thinnest reference deposit would be most sensitive to start up phenomena such as the deposition not beginning at precisely the same time as the timer started and the effects of deposit forming on a clean tube. It is likely that the deposition rate would be lower when the deposit is forming on a clean tube than a carbon coated one, leading

to a lower than expected deposit thickness. The percent difference would also be most sensitive to discrepancies in this case because each nanometer of film is a larger portion of the whole for the thinnest deposit. The reportedly 90 nm reference tube was also not particularly well matched. The models measured 60 nm for this tube. This sample is unique in that its visual appearance does not appear to follow the trend of the others. Several of the other reference tubes have gray deposits on them that grow darker visually as the deposit grows thicker. The 90 nm tube appears very light, lighter than several of the tubes that have reportedly thinner deposits, which seems out of place. In fact, the appearance of this tube is quite similar to the one marked with a 60 nm thickness. The 90 nm reference tube is second from the bottom in the figure below. The 60 nm tube is fourth from the bottom, and the one between them is 75 nm. Although the eye is very insensitive to these types of changes, and these reports cannot be used with any certainty, it seems odd that this tube does not follow the pattern of the others, and this is enough to call into question the theoretically known thickness in this case, especially given that the model is successful in predicting the other reference tube thicknesses. Figure 30 shows the reference tubes in order of increasing theoretical deposit thickness.

Figure 30: Reference tubes with theoretically known deposit thicknesses

The final step in the model evaluation process was determining the best substrate to match the reference tubes. A reference material was originally used in the modeling, and this yielded acceptable results. Then, a data point from the clean section of one of the tubes was used, which was better than the reference material. The best substrate was ultimately specific to each tube. The clean sections of the tubes were modeled using the reference aluminum and aluminum oxide model, then the point where the mean aluminum oxide layer thickness occurred was used as the substrate for that tube. Since this section of the tube was covered with Kapton tape during the deposition, there is no possibility that the film layer is carbon, and it must be aluminum oxide. This yielded the closest matches for all of the reference tubes.

In finding the best model to match the reference tube results, an important discovery about the optical constants of the film was made. Originally, the new amorphous dispersion was used to represent the films on the aluminum substrates. This dispersion follows the optical constants published for the films in the ASTM D3241 standard for determining thermal stability. These

values are n equal to 1.45 and k equal to 0 at a wavelength of 1550 nm. It was found through the investigation process though that the Tauc-Lorentz dispersion was able to represent the values of the known deposit thicknesses better than the new amorphous dispersion, which is why the Tauc-Lorentz was chosen to model all of the samples presented in the results sections. This is visualized in Figure 29. The Tauc-Lorentz dispersion used here gives n equal to 2.3 and k equal to 0 at the same wavelength. This suggests that the published optical constant values given in the standard may need to be revisited, and better values may be obtainable. Single values for the index of refraction and coefficient of extinction are published in the standard instead of spectra for the ellipsometric tube rater because the ETR uses only one wavelength of light. This also means that the ETR cannot fit the optical constants, only the deposit thickness. The result obtained here raises questions as to whether such an instrument can accurately define a deposit when it is restricted to single optical constants, and whether the published optical constants are best for all films.

Scanning Electron Microscopy Validation

Scanning Electron Microscopy (SEM) data was taken on two of the aluminum tubes that were exposed to Sasol IPK in an attempt to validate the ellipsometric thickness measurements. The tubes were cut to expose their circular cross sections so that the depth of the deposit could be viewed around the circumference of the tube. Each tube was cut into several sections to mimic how the thickness measurements were made with the ellipsometer along the tube's length. Figure 31 shows how the tubes were cut in preparation for the SEM analysis.

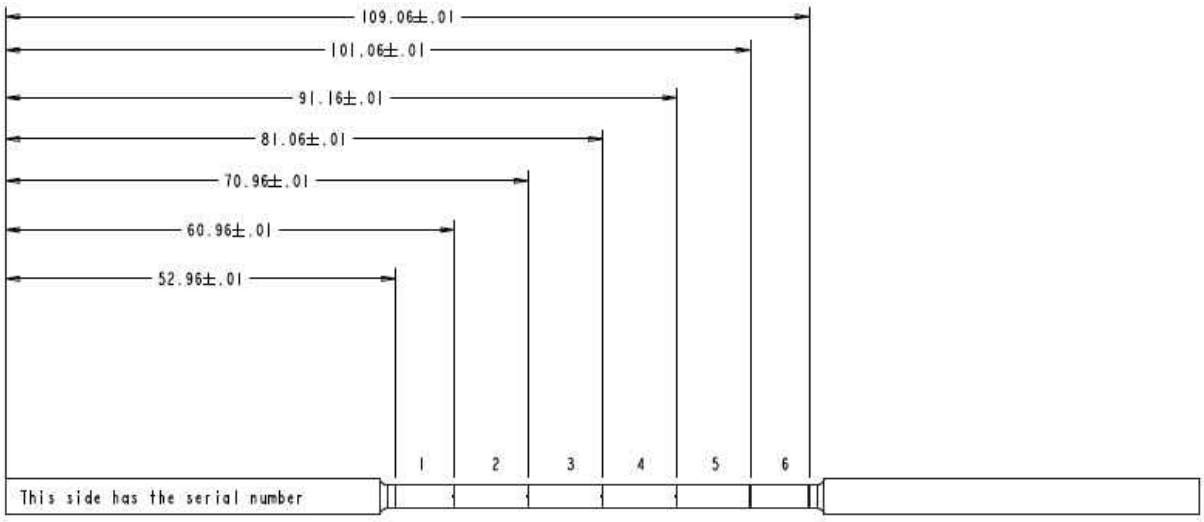

Figure 31: Cutting locations for SEM

Scanning electron microscopy allows highly magnified pictures of surfaces to be taken. In this work, a 15,000 times magnification was used. The tube sections were mounted upright in holding cylinders which were then filled with epoxy to keep them in place. The cross-sectional surface that was to be examined was carbon coated to eliminate charging in the image. One issue with this method was that the mounting epoxy shrank as it dried and pulled the deposit away from the tube surface. This made it difficult to determine the starting and ending points of the deposit, and it also makes it impossible to be sure that the thickness being measured by the SEM is the same as it was before the sample was damaged. It cannot be said with certainty that the deposit was not stretched or otherwise deformed when it was pulled away. It is likely that some of the deposit stayed on the tube surface and the rest was stuck to the mounting epoxy. Figure 32 shows one of the images taken by the SEM. Point A is well within the aluminum substrate, B is either the surface of the substrate or part of the deposit, points C, D, and E are within the deposit, and points

F and G are within the mounting epoxy. The void where the deposit was pulled away from the tube is visible as the black strip between points B and C.

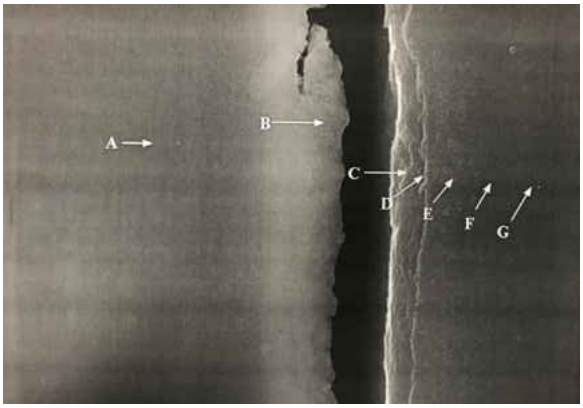

Figure 32: SEM results

Compositional analysis was also performed at each labeled point using Energy Dispersive X-ray Spectroscopy (EDS). This technique involves exciting the sample with x-rays and using the energy spectrum that results to identify its composition. Point A, well within the substrate showed mostly aluminum, as would be expected since it was an aluminum tube, and trace amounts of carbon and magnesium. At point B where the epoxy shrank away the composition is mostly still aluminum, with relatively higher, but still low levels of carbon, and trace elements of magnesium, silicon, and chlorine. Chlorine is contained in the mounting epoxy, so it is likely that some of the matrix permeated the deposit, possibly dissolving it into the rest of the mounting material. Across the void at point C, the composition is still mostly aluminum, with significant levels of carbon, and still trace amounts of magnesium, oxygen, silicone, and chlorine. This point is most likely in the aluminum oxide layer that was under the deposit layer. At point D, the composition becomes more and more carbon intense, with less aluminum. The aluminum finally disappears far into the

mounting material, where only carbon is present. It is difficult to say at what point between the void and the mounting material the deposit starts and stops. The spectrum from point C is shown in Figure 33.

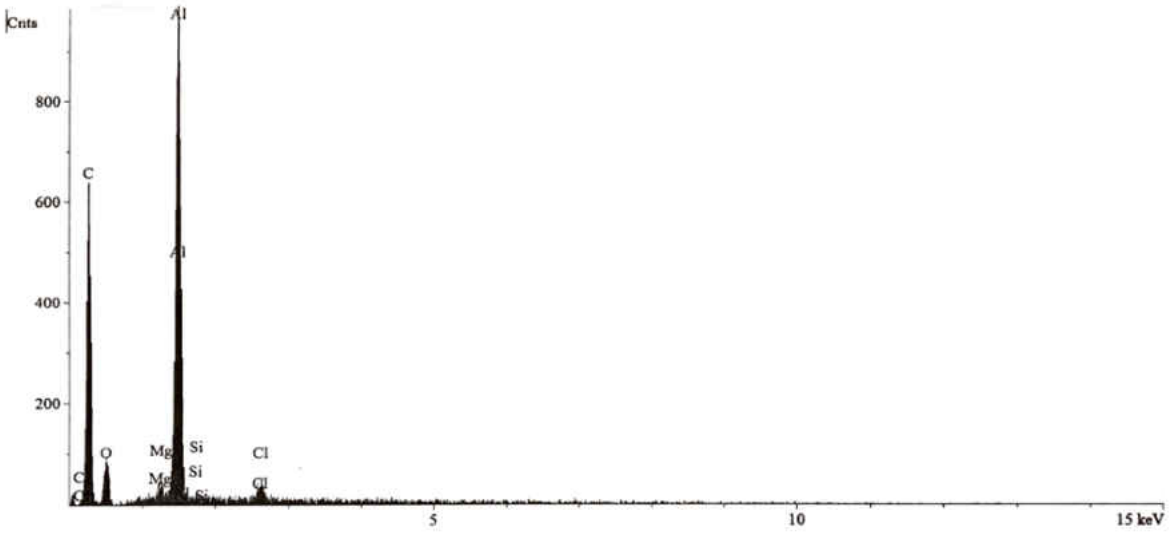

Figure 33: EDS analysis for point C

Originally, this effort was made in an attempt to validate the ellipsometric thickness measurements, however due to the complications that arose, it is not possible to definitively verify the measurements in this way. The fact that the deposit could have been damaged between the time when the ellipsometric measurement was taken and when the SEM analysis was performed prevents validation in this way. If SEM was to be done in the future for this same application, it is recommended that the tubes with deposit on them be coated in platinum and then nickel plated in order to provide separation between the deposit and the mounting material. This would prevent any interaction between the mount and the deposit, and would likely stop the deposit from being pulled away from the substrate. While these results cannot be used for their original purpose, some

commentary about the effectiveness of SEM versus ellipsometry as a thermal stability measurement alternative is possible. It has been suggested that SEM might have been an alternative to ellipsometry for measuring deposit thicknesses. It seems appealing to be able to examine the deposits directly instead of having to use optical models. To perform the SEM properly, an investment of time and money would have to be made, and even then, unforeseen complications may arise. For instance, it is not possible at this point to be sure that cutting the tubes into sections did not damage the deposit. For these reasons, ellipsometry is a better alternative than SEM for measuring the thicknesses of these deposits to characterize thermal stability. Ellipsometry does not involve altering the deposits in any way, and thus does not risk damaging them or affecting the results.

Ellipsometric Tube Rater Validation

Another attempt to validate the ellipsometric measurements was made using the Ellipsometric Tube Rater (ETR) from Wright Patterson Air Force Base. Zachary West and Tim Edwards aided in this effort. Four of the stainless steel tubes were analyzed using the ETR and the thickness profiles were compared to those from the ellipsometer. The ellipsometer and ETR are related instruments, in that both use the principles of ellipsometry to determine film thickness. The ETR also has the capability to scan the entire tube surface to obtain thickness profiles around the circumference of the tube. One benefit of the ellipsometer over the ETR is that the ellipsometer is spectroscopic, using light that covers a range of wavelengths, while the ETR uses only a single wavelength of light. This means that the ETR can only be used to determine deposit thicknesses, and cannot also determine film composition or optical constants. It is limited to using the index of

refraction and coefficient of extinction of the film and substrate given by the ASTM D3241 standard for thermal stability. These values are not always the most accurate for a film or substrate, and the ellipsometer can compensate for this by determining the actual values. This does make the ellipsometric modeling and analysis more time consuming and in depth, but in cases where the optical constants of the film or substrate are not confidently known, this extra effort can be justified. On the other hand, for routine thermal stability testing, in the cases where the index of refraction and coefficient of extinction of the substrate and deposit match the published values well, the ETR provides a quick automated way to determine the maximum deposit thickness and profile.

The shapes of the profiles measured by the ellipsometer and the ETR show excellent agreement, however the magnitudes of the thicknesses do not agree. In all cases, there is greater than 100 percent difference between the values measured by the ellipsometer and those measured by the ETR. When the ETR data is normalized by its lowest value, the agreement in thickness magnitudes is much more satisfactory. Normalization was done by subtracting the minimum value of the deposit thickness measured by the ETR from every other data point. The ETR generally does this normalization automatically, however because the films on these tubes were quite thick and near the instrument's saturation limit the ETR had difficulty in determining the correct offset to apply, and this had to be done manually. The various profiles for an example tube are shown in Figure 34. This allows confidence to be had in the ellipsometric model measurements for the stainless steel cases.

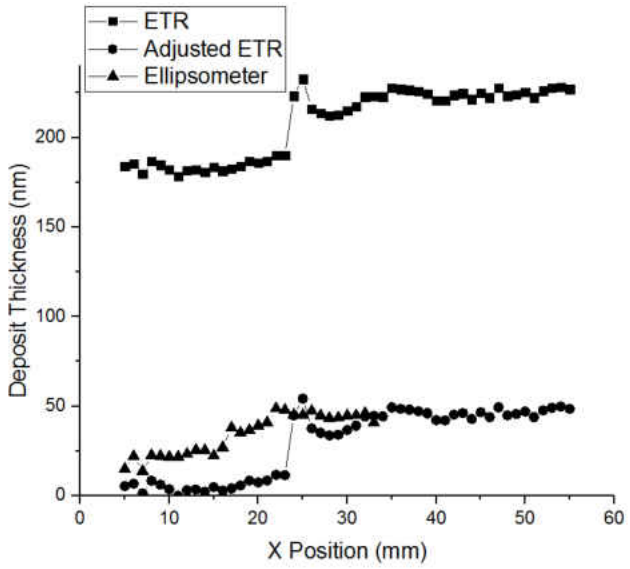

Figure 34: Stainless steel tube 1311 comparison of ETR and ellipsometric data

Interferometric Tube Rater Validation

The aluminum tube measurements were compared to measurements made using the Interferometric Tube Rater (ITR) from Wright Patterson Air Force Base, again with the help of Zachary West and Tim Edwards. The ITR uses interferometry, in which a single beam of unpolarized light is split into two halves. One half never encounters the sample and the other reflects from it. The ITR uses interference patterns produced when these two beams are overlaid to determine the thickness of the film on the sample. Three of the aluminum tubes exposed to Sasol IPK were analyzed in this way, and the results were compared to those obtained by the ellipsometer. The shapes of these thickness profiles do not match particularly well, but the magnitudes of the maximum deposit thicknesses do show close agreement. Two of the three tubes match within 6 nm of each other in terms of maximum deposit thickness. The ITR uses optical constant spectra to model the substrates and deposits. Different spectra were used by the

ellipsometer for reasons that are given in the reference tube validation section. This may explain the differences in the thickness profile shapes that are seen for all three of the tubes compared in this way. A summary of the ITR results is shown in Table 5.

Table 5: ITR comparisons

Tube	Ellipsometer Maximum Thickness (nm)	ITR Maximum Thickness (nm)	Percent Difference
1291	84.40	81.13	3.95
1293	70.68	47.70	38.83
1251	43.60	48.27	10.17

A sample comparison of the ITR and ellipsometric thickness profiles is shown below in Figure 35 and Figure 36. Some of the differences between the two methods can also be accounted for by the fact that the ellipsometry data was taken at 2 mm intervals along the tube length while the ITR data was taken at smaller intervals, resulting in better resolution of the deposit profile shape.

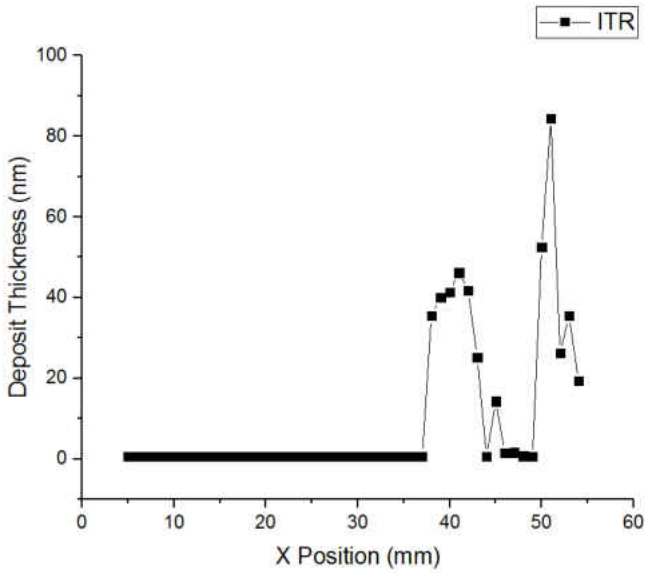

Figure 35: ITR thickness profile

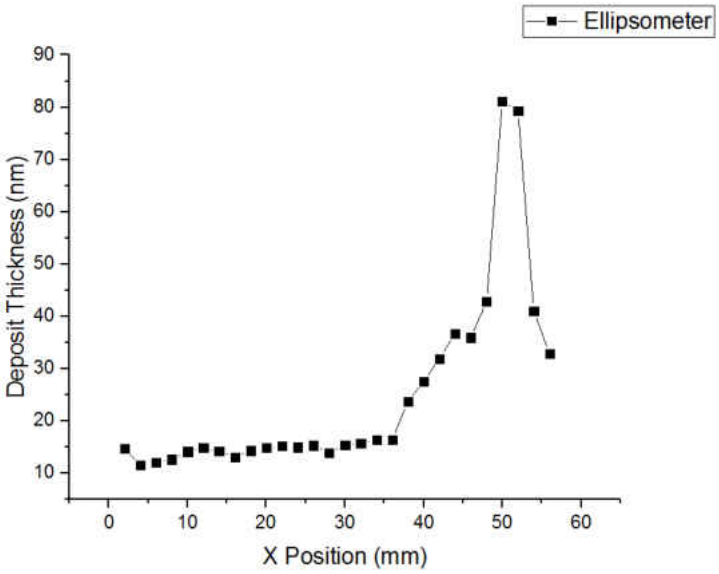

Figure 36: Ellipsometric thickness profile

Recommendations

There is currently interest in the thermal stability community in revising the current ASTM standard for stability characterization and testing. Based on the work that has been carried out here, several recommendations can be made for the improvement of the standard. First, it is recommended that deposit volume be added as a thermal stability test metric, either in addition to maximum thickness or as a replacement criterion. As was shown in the Sasol IPK results sections, maximum deposit thickness is not always indicative of the total amount of deposit present, and ultimately the total deposit impacts the engine performance more than a single point with high levels of deposition.

Secondly, the results of this work support the removal of the color standard from the thermal stability test method altogether. The results of the Gevo color comparisons with the ellipsometric ratings demonstrate the imprecision of the color standard and the way that deposit color is not necessarily indicative of deposit thickness. Currently, ellipsometry is included in an appendix to the standard test method as an acceptable alternative to the color standard, but the color test is still included in the main body of the method. Given the results of this test showing that ellipsometry is much more detailed than the color test, it is recommended that the color standard not be used for thermal stability testing.

Finally, it is recommended that the optical constants published in the ASTM standard for modeling carbon films be revisited. These values did not accurately model the samples in this work, as demonstrated in the reference tube section. It is possible that these values are unable to capture all carbon films, and adjustments to the standard should be made.

CHAPTER FIVE: CONCLUSION

Thermal stability is an important characteristic of a jet fuel to understand. Jet fuel is often used as engine coolant to save weight and space, and a significant challenge that must be overcome in the future will be the ability of the fuel to absorb the heat produced by the aircraft's engine. Thermally unstable fuels are unable to absorb enough heat to allow the engine to function properly, and the deposits they form can lead to fuel flow losses and fouling. Thermal stability must be characterized before a fuel can be used in an actual aircraft.

Ellipsometry has previously been added to the thermal stability characterization method because it improves over the color standard in many ways. It is objective, repeatable, quantitative, precise, nondestructive, and versatile. The color standard on the other hand, was subjective, non-repeatable, limiting, and qualitative. The level of detail that can be resolved using an ellipsometer is enormously higher than what can be seen using the color standard which relies on the capabilities of the human eye. The addition of ellipsometry to the test standard was an enormous improvement to thermal stability testing.

Alternative fuels will be important to all sectors of energy generation in the future, including aviation. Alternative fuels are often cleaner burning than traditional fuels, and they will help secure the world's energy resources into the future. Diverse and reliable energy sources are important to this future, and alternative fuels will help fill this need.

Various tests have been done previously using ellipsometry, as detailed in previous chapters. Ellipsometry has been used to measure the deposition profiles of a few traditional fuels in previous works, and limited work has been done on alternative fuels. Various tests for thermal stability and deposition behavior, including isothermal flow reactors and quartz crystal

microbalance experiments have also been performed, but ellipsometry is better in many ways. Ellipsometry is nondestructive and quick, allowing all batches of fuel to be tested in an industrial application.

The Hot Liquid Process Simulator was used to expose the tubes to the fuels. The tube was resistively heated and the fuel was flowed over it. Then the tube was cooled and analyzed in the ellipsometer. This was done according to the ASTM thermal stability testing standards. Ellipsometric principles were used to determine the thickness of the deposits left by the heated jet fuels on the tubes. At an interface between two materials, an incoming beam of light reflects and refracts according to Snell's Law. The Fresnel Relations are used to track the changes in intensity and phase of the light as it interacts with the sample. The ellipsometer measures the parameters Δ and Ψ to characterize the sample.

Theoretical optical models were investigated and used to match the experimental data to determine the deposit thickness. Models that fit only the deposit thickness were found to produce profiles that were more realistic than the ones that fit both thickness and optical constants. It was concluded that models fitting several parameters were too flexible, and were trying to fit the noise in the data. Reference materials for aluminum and aluminum oxide were used to model clean tubes that had not been exposed to the fuel in order to find a realistic substrate for subsequent models. The new amorphous dispersion representation of the optical constants was tested but ultimately found to not produce the correct magnitudes of the deposit thickness when they were applied to the reference tubes. The Tauc-Lorentz formula was found to be the best fit for this application because it matched the most reference tubes the closest and yielded plausible thickness profiles. This finding was interesting because this dispersion used different optical constant curves than what are published in ASTM D3241, and suggests that more investigation is needed to determine

which are the better values for all carbon films. In order to model the tubes most accurately, "self substrates" were used. For the reference tubes, the data point on the clean sections of the tube that had the median aluminum oxide thickness as modeled by the reference material model was used for the substrate. This could be done because the clean sections of the tube were covered during deposition, so the layer was certainly aluminum oxide. This was done for each individual reference tube and for a few clean tubes, and a representative data point was chosen as the substrate for all of the tubes exposed to the jet fuels. Roughness layers were implemented on all of the models, but the additional flexibility did not change the measured thicknesses and only marginally reduced the χ^2 values, so a roughness layer was not used in the final model.

Several attempts were made to validate the ellipsometric thickness measurements. An SEM study was undertaken on two of the tubes, in which the tubes were cut to expose their cross sections so that highly magnified pictures of the deposit layer around the tube circumference could be taken. Several issues arose in trying to validate the measurements in this way, and while this prevented the results from being used to validate the ellipsometric findings, it does support the use of ellipsometry over SEM as a thermal stability characterization method. ITR data was also taken on several of the aluminum tubes by researchers at WPAFB. This data showed good agreement in the maximum thicknesses on the tubes, but some discrepancies in the deposit profile shapes. This was attributed to the two instruments using different sets of optical constants. ETR data was taken on a few of the stainless steel tubes, and these results showed very good agreement in the profile shapes, but differences in the thickness magnitudes. When the minimum deposit thickness was subtracted from each profile point measured by the ETR, the agreement was much better. This was attributed to incorrect normalization of the ETR data. Lastly, the models were validated using reference tubes with known deposit thicknesses on them. The Tauc-Lorentz model was found to

match most of the reference tubes well with a few exceptions. In these cases, it is possible that the reported deposit thicknesses were incorrect.

Several fuel studies were performed using ellipsometry to quantify thermal stability and deposition behavior. Several batches of Jet A were studied to observe the differences in deposition at 260 °C. Most of the results clustered at the lower deposition levels, but some existed well outside of the normal range. The effects of increasing temperature and increasing naphthalene concentration were assessed on aluminum and stainless steel tubes exposed to Sasol IPK. In several instances, it was noted where the deposit volume instead of the maximum deposit thickness was more indicative of the fuel's thermal stability. The repeatability of the measurement was also discussed. Gevo jet fuel was assessed in terms of increasing temperature, and it was found that the deposition stayed almost constant, or increased very slowly up to a particular temperature, and then increased much more rapidly. This was in agreement with the observed behavior for JP-8 and literature findings for other fuels. The Gevo tubes also provided an opportunity to compare the color standard and ellipsometry. Several cases were noted where a tube failed the color standard test, but passed the ellipsometric test for thermal stability. Cases were also noted where tubes with lower deposit thicknesses were given higher color standard ratings, meaning that they were more thermally stable than the color standard predicted. This highlights the improvement of ellipsometry over the previously used color standard.

Three recommendations are made for the improvement of the ASTM thermal stability standard based on this work. First, deposit volume should be added as a test criterion for thermal stability. Next, the color standard should be completely removed from the method, and finally, the published optical constants for carbon films should be revisited.

Several lessons were learned over the course of this work that could be important in its continuation. First, more satisfactory SEM results could have been obtained if the deposit had not been pulled away from the substrate by the mounting epoxy. If this was done again, it is recommended that the samples be platinum sputter coated, then plated with nickel. This would be more time consuming and expensive, however it would keep the entire sample intact. It would also make the determination of the starting and stopping point of the deposit more straightforward. The heavy platinum would provide a clear boundary because it of its weight, making it appear very distinct from the deposit in the SEM images.

Next, an effective method for testing various models was found through a great deal of trial and error. First, different films should be tested on a constant substrate. Several different dispersions should be tested in this phase because unexpected models may be best for a particular situation. Then, different substrates should be tested with the best film. These should include a reference material and a self-substrate if possible. Lastly, a roughness layer should be tested.

Finally, and possibly most importantly, the tubes should be analyzed with the ellipsometer prior to their exposure to the fuel in order to be able to account for surface roughness and differing oxide thickness layers. Ideally, each point along the tube should be modeled with the same clean point as the substrate. This would increase modeling time because each point of each tube would need to have its own model, but this method would provide the most accuracy. Alternatively, only points that are outliers in some way could be modeled in this way as a compromise between speed and accuracy.

In the future, this work could be extended to other fuels, substrates, and additives. In theory, any combination that yields relatively thin deposits (<300 nm) could be analyzed by ellipsometry. Additionally, wider temperature ranges and more repeatability tests could be explored. More SEM

analysis could be done to definitively validate the thickness measurements. Lastly, all of this data could be incorporated into a predictive model or database for deposition. This would require extensive testing and repeatability testing of all fuels of interest, but would be useful to researchers and fuel users alike.

Thermal stability is an important aspect of a jet fuel's behavior to understand. It directly impacts engine performance, and has the possibility to cause failure if not properly managed. Ellipsometry is a powerful tool for understanding a fuel's thermal stability, providing a wealth of detail that is useful in analysis. Ellipsometry will continue to be more widely used in the future, and the knowledge obtained using this technique will be invaluable to the operation and design of future engines.

APPENDIX A: SASOL IPK DATA

Table 6: Aluminum Sasol IPK Data

Tube Number	Test Temperature (°C)	Fuel	Average χ^2	Thickness Pass/Fail	Max thickness (nm)	Deposit Volume (mm^3)	JFTOT Color Pass/Fail
1304	300	N118 SASOL IPK (100 %vol)	45.2	P	17.62	0.0050	1 (P)
1305	320	N118 SASOL IPK (100 %vol)	22.5	P	9.18	0.0033	1 (P)
1306	360	N118 SASOL IPK (100 %vol)	46.6	P	19.61	0.0065	1 (P)
1310	380	N136 SASOL IPK-1-M-Napthalene (99-1 %vol)	137.8	P	29.14	0.0103	1 (P)
1321	300	N138 SASOL IPK-1-M-Napthalene (95-5 %vol)	12.5	P	10.04	0.0031	1 (P)
1322	300	N138 SASOL IPK-1-M-Napthalene (95-5 %vol)	31.8	P	21.66	0.0053	<2 (P)
1327	380	N139 SASOL IPK-1,2,3,4-T-Napthalene (97-3 %vol)	68.8	P	24.23	0.0073	1 (P)
1330	345	N140 SASOL IPK-1,2,3,4-T-Napthalene (97-3 %vol)	121.9	P	28.80	0.0092	1 (P)
1335	380	N118 SASOL IPK (100 %vol)	21.6	P	11.61	0.0035	1 (P)
1337	380	N136 SASOL IPK-1-M-Napthalene (99-1 %vol)	42.4	P	21.41	0.0057	1 (P)
1344	340	N137 SASOL IPK-1-M-Napthalene (97-3 %vol)	1.2	P	3.60	0.0007	1 (P)

Table 7: Stainless Steel Sasol IPK Data

Tube Number	Test Temperature (°C)	Fuel	Average χ^2	Thickness Pass/Fail	Max thickness (nm)	Deposit Volume (mm^3)	JFTOT Color Pass/Fail
1308	390	N118 SASOL IPK (100 %vol)	90.7	P	38.34	0.0155	4 (F)
1309	385	N118 SASOL IPK (100 %vol)	29.4	P	33.49	0.0102	3 (F)
1311	385	N136 SASOL IPK-1-M-Napthalene (99-1 %vol)	147.9	P	48.43	0.0187	4 (F)
1328	400	N139 SASOL IPK-1,2,3,4-T-Napthalene (99-1 %vol)	203.4	P	58.55	0.0222	4 (F)
1329	385	N139 SASOL IPK-1,2,3,4-T-Napthalene (99-1 %vol)	126.6	P	63.60	0.0194	4 (F)
1332	385	N140 SASOL IPK-1,2,3,4-T-Napthalene (97-3 %vol)	264.4	P	64.66	0.0209	4 (F)
1333	385	N141 SASOL IPK-1,2,3,4-T-Napthalene (95-5 %vol)	330.6	P	65.02	0.0224	4 (F)
1339	385	N136 SASOL IPK-1-M-Napthalene (99-1 %vol)	29.4	P	33.49	0.0102	3 (F)

APPENDIX B: GEVO DATA

Table 8: Aluminum Gevo Data Summary

Tube ID	Fuel	Test Temperature (°C)	Composition	Color Rating	Max Thick (nm) Pos 1	Max Thick (nm) Pos 3	Volume Pos 1 (mm^3)	Volume Pos 3 (mm^3)
1229	N81 GEVO	290	100	2	5.05	6.79	0.0017	0.0027
1230	N81 GEVO	320	100	2	5.45	6.26	0.0017	0.0010
1231	N81 GEVO	330	100	1	4.56	5.26	0.0017	0.0020
1234	N81 GEVO	350	100	1	8.59	4.93	0.0022	0.0016
1235	N81 GEVO	375	100	<2	34.70	41.93	0.0077	0.0098
1238	N81 GEVO	380	100	<2	28.96	17.39	0.0055	0.0054
1250	N93 Jet A	260	100	3	111.02	133.06	0.0103	0.0074
1251	N93 Jet A	250	100	1	20.65	19.05	0.0038	0.0040
1257	N81 GEVO	380	100	<2	21.07	18.47	0.0069	0.0064
1260	N81 GEVO	375	100	2	11.35	10.05	0.0041	0.0037
1261	N98 GEVO-JP8	300	75-25	1	7.45	8.08	0.0030	0.0034
1262	N81 GEVO	380	100	1	10.65	13.19	0.0031	0.0034
1263	N98 GEVO-JP8	310	75-25	1	9.46	28.55	0.0029	0.0047
1271	N98 GEVO-JP8	330	75-25	<3	57.95	44.06	0.0085	0.0078
1272	N98 GEVO-JP8	335	75-25	<4	50.39	28.76	0.0068	0.0061
1273	N99 GEVO-JP8	335	80-20	2	35.72	18.71	0.0060	0.0050
1274	N99 GEVO-JP8	345	80-20	<4	15.68	48.82	0.0048	0.0064
1275	N99 GEVO-JP8	340	80-20	<4	13.06	21.82	0.0041	0.0052
1277	N100 GEVO-JP8	335	85-15	1	16.55	16.73	0.0073	0.0076
1278	N100 GEVO-JP8	340	85-15	1	13.96	13.95	0.0045	0.0046

Tube ID	Fuel	Test Temperature (°C)	Composition	Color Rating	Max Thick (nm) Pos 1	Max Thick (nm) Pos 3	Volume Pos 1 (mm^3)	Volume Pos 3 (mm^3)
1279	N100 GEVO-JP8	350	85-15	2	33.33	29.39	0.0085	0.0085
1281	N100 GEVO-JP8	360	85-15	2	16.71	14.64	0.0059	0.0054
1282	N100 GEVO-JP8	355	85-15	1	13.78	13.52	0.0052	0.0049
1283	N101 GEVO-JP8	360	90-10	<2	8.06	9.63	0.0026	0.0030
1284	N101 GEVO-JP8	370	90-10	1	17.82	21.67	0.0082	0.0088
1286	N101 GEVO-JP8	380	90-10	1	13.54	12.10	0.0047	0.0045
1288	N102 GEVO-JP8	380	95-5	1	11.80	13.44	0.0038	0.0046

Table 9: Stainless Steel Gevo Data Summary

Tube ID	Fuel	Test Temperature (°C)	Composition	Color Rating	Max Thick (nm) Pos 1	Max Thick (nm) Pos 3	Volume Pos 1 (mm^3)	Volume Pos 3 (mm^3)
1237	N81 GEVO	390	100	>4	54.48	56.45	0.0186	0.0187
1239	N81 GEVO	385	100	>4	53.83	56.66	0.0185	0.0189
1268	N81 GEVO	385	100	>4	58.13	58.41	0.0188	0.0182
1287	N101 GEVO-JP8	385	90-10	4	49.08	46.63	0.0202	0.0188
1289	N102 GEVO-JP8	385	95-5	>4	50.28	48.45	0.0193	0.0193

APPENDIX C: JP-8 DATA

Table 10: JP-8 Data Summary

Tube ID	Fuel	Test Temperature (°C)	Composition	Color Rating	Max Thick (nm) Pos 1	Max Thick (nm) Pos 3	Volume Pos 1 (mm^3)	Volume Pos 3 (mm^3)
1232	N84 JP8	270	100	0	6.95	6.45	0.0027	0.0029
1233	N84 JP8	290	100	1	11.88	12.52	0.0029	0.0032
1241	N84 JP8	300	100	2	29.33	23.77	0.0049	0.0039
1243	N84 JP8	305	100	<4	74.62	119.98	0.0093	0.0135
1254	N84 JP8	300	100	<3	69.16	63.48	0.0085	0.0084
1256	N84 JP8	305	100	<4	134.03	89.56	0.0145	0.0137

APPENDIX D: JET A DATA

Table 11: Jet A Data Summary

Tube ID	Fuel	Test Temperature (°C)	Composition	Color Rating	Max Thick (nm) Pos 1	Max Thick (nm) Pos 3	Volume Pos 1 (mm^3)	Volume Pos 3 (mm^3)
1250	N93 Jet A	260	100	3	111.02	133.06	0.0103	0.0074
1252	N94 Jet A	260	100	1	10.28	10.41	0.0028	0.0029
1253	N96 Jet A	260	100	1	9.54	8.72	0.0019	0.0019
1255	N97 Jet A	260	100	1	3.63	4.21	0.0011	0.0012
1258	N105 Jet A	260	100	1	4.80	4.52	0.0015	0.0014
1265	N107 Jet A	260	100	1	7.49	4.39	0.0021	0.0019
1266	N108 Jet A	260	100	1	9.52	10.05	0.0026	0.0026
1267	N109 Jet A	260	100	1	12.94	14.57	0.0033	0.0035
1291	N122 Jet A	260	100	>3	19.22	19.01	0.0051	0.0050
1292	N124 Jet A	260	100	<2	9.20	14.61	0.0024	0.0032
1293	N125 Jet A	260	100	1	18.98	19.36	0.0045	0.0048
1303	N131 jet A	260	100	1	53.54	19.83	0.0043	0.0041
1343	N142 Jet A	260	100	4P	81.99	121.71	0.0084	0.0136

LIST OF REFERENCES

[1] Colket, M. B., Heyne, J., Rumizen, M., Edwards, J. T., Gupta, M., Roquemore, W. M., Moder, J. P., Tishkoff, J. M., and Li, C., "An overview of the national jet fuels combustion program," Proc. 54th AIAA Aerospace Sciences Meeting, p. 0177.

[2] "U.S. Coal Reserves," https://www.eia.gov/coal/reserves/.

[3] ASTM Standard D4054-14, 2015, "Standard Practice for Qualification and Approval of New Aviation Turbine Fuels and Fuel Additives," ASTM International, West Conshohocken, PA, 2003, www.astm.org.

[4] ASTM Standard D7566, 2015, "Standard Specification for Aviation Turbine Fuel Containing Synthesized Hydrocarbons," ASTM International, West Conshohocken, PA, 2003, www.astm.org.

[5] ASTM Standard D3241, 2015, "Standard Test Method for Thermal Oxidation Stability of Aviation Turbine Fuels (JFTOT Procedure)," ASTM International, West Conshohocken, PA, 2003, DOI:10.1520/D3241-08, www.astm.org.

[6] Baker, C., David, P., Taylor, S., and Woodward, A., "Thickness measurement of JFTOT tube deposits by ellipsometry," Proc. Proceedings of the 5th International Conference on Stability and handling of liquid fuels, Department of Energy Washington, DC, pp. 433-447.

[7] Moses, C. A., 2008, "Comparative evaluation of semi-synthetic jet fuels," Contract, 33415(02-D), p. 2299.

[8] Hui, X., Kumar, K., Sung, C.-J., Edwards, T., and Gardner, D., 2012, "Experimental studies on the combustion characteristics of alternative jet fuels," Fuel, 98, pp. 176-182.

[9] Dryer, F. L., Ju, Y., Brezinsky, K., Santoro, R. J., Litzinger, T. A., and Sung, C.-J., 2012, "Generation of Comprehensive Surrogate Kinetic Models and Validation Databases for Simulating Large Molecular Weight Hydrocarbon Fuels," DTIC Document.

[10] Lindsey, J., and Klettlinger, S., 2013, "Thermal Stability Results of a Fischer-Tropsch Fuel With Various Blends of Aromatic Solution."

[11] Corporan, E., Edwards, T., Shafer, L., DeWitt, M. J., Klingshirn, C., Zabarnick, S., West, Z., Striebich, R., Graham, J., and Klein, J., 2011, "Chemical, thermal stability, seal swell, and emissions studies of alternative jet fuels," Energy & Fuels, 25(3), pp. 955-966.

[12] Zabarnick, S., 1994, "Studies of jet fuel thermal stability and oxidation using a quartz crystal microbalance and pressure measurements," Industrial & engineering chemistry research, 33(5), pp. 1348-1354.

[13] Altin, O., and Eser, S., 2001, "Analysis of solid deposits from thermal stressing of a JP-8 fuel on different tube surfaces in a flow reactor," Industrial & engineering chemistry research, 40(2), pp. 596-603.

[14] Lauer, J. L., and Vogel, P., 1984, "Emission FTIR analyses of thin microscopic patches of jet fuel residues deposited on heated metal surfaces," Applications of Surface Science, 18(1-2), pp. 182-206.

[15] Pande, S., Hardy, D., Kamin, R., Nowack, C., Colbert, J., Morris, R., and Salvucci, L., 2001, "Quest for a reliable method for determining aviation fuel thermal stability: Comparison of turbulent and laminar flow test devices," Energy & fuels, 15(1), pp. 224-235.

[16] Grinstead, B., and Zabarnick, S., 1999, "Studies of jet fuel thermal stability, oxidation, and additives using an isothermal oxidation apparatus equipped with an oxygen sensor," Energy & fuels, 13(3), pp. 756-760.

[17] Zabarnick, S., and Mick, M., 1999, "Inhibition of jet fuel oxidation by addition of hydroperoxide-decomposing species," Industrial & engineering chemistry research, 38(9), pp. 3557-3563.

[18] Heneghan, S. P., and Zabarnick, S., 1994, "Oxidation of jet fuels and the formation of deposit," Fuel, 73(1), pp. 35-43.

[19] Bessee, G. B., Wilson III, G. R., and O'Brien, S., 2012, "Storage Stability of Jet Fuel Not Containing Anti-Oxidant (AO)," DTIC Document.

[20] Altin, O., and Eser, S., 2004, "Carbon deposit formation from thermal stressing of petroleum fuels," Am. Chem. Soc. Div. Fuel Chem, 49, pp. 764-766.

[21] Zabarnick, S., 1993, "Chemical kinetic modeling of jet fuel autoxidation and antioxidant chemistry," Industrial & engineering chemistry research, 32(6), pp. 1012-1017.

[22] Klettlinger, J. L. S., 2012, "Effect of Aromatic Concentration of a Fischer-Tropsch Fuel on Thermal Stability."

[23] Edwards, T., DeWitt, M. J., Shafer, L., Brooks, D., Huang, H., Bagley, S. P., Ona, J. O., and Wornat, M. J., "Fuel composition influence on deposition in endothermic fuels," Proc. 14th AIAA/AHI Space Planes and Hypersonic Systems and Technologies Conference, Canberra, Australia.

[24] Browne, S. T., Wong, H., Hinderer, C. B., and Klettlinger, J., 2012, "Enhancement of Aviation Fuel Thermal Stability Characterization Through Application of Ellipsometry."

[25] Tompkins, H. G., and McGahan, W. A., 1999, Spectroscopic ellipsometry and reflectometry: a user's guide, Wiley.

[26] Horiba Jobin Yvon, "Spectroscopic Ellipsometry User Guide," 2008.

[27] Horiba AutoSE System User Manual, Part No. 31087139, France, March 2009.

[28] Alcor-PAC, 2003, "Hot Liquid Process Simulator (HLPS 400) User's Manual Rev. B," Oct. 2003, Version 5

[29] "New Amorphous Dispersion Formula," TN 12, Horiba, Nov. 2006.

[30] "Tauc-Lorentz Dispersion Formula," TN 11, Horiba, Nov. 2006.

[31] Horiba Scientific, "DeltaPsi2 Software Reference Manual," 2009.